University of Pittsburgh

An Effective Quality Assurance Method for Additively Manufactured Gas Turbine Metallic Components via Machine Learning from In-Situ Monitoring, Part-scale Modeling, and Ex-Situ Characterization Data

Presented to: NETL –UTSR Review Workshop 2020

PI: Dr. Xiayun Zhao
Co-PIs: Dr. Albert To (Pitt), Dr. Richard Neu (GaTech)

Department of Mechanical Engineering and Materials Science
University of Pittsburgh

November 17th, 2020

Laser Powder Bed Fusion (LPBF) based Metal Additive Manufacturing (AM)

Video Source: Siemens (LPBF for Gas Turbine)

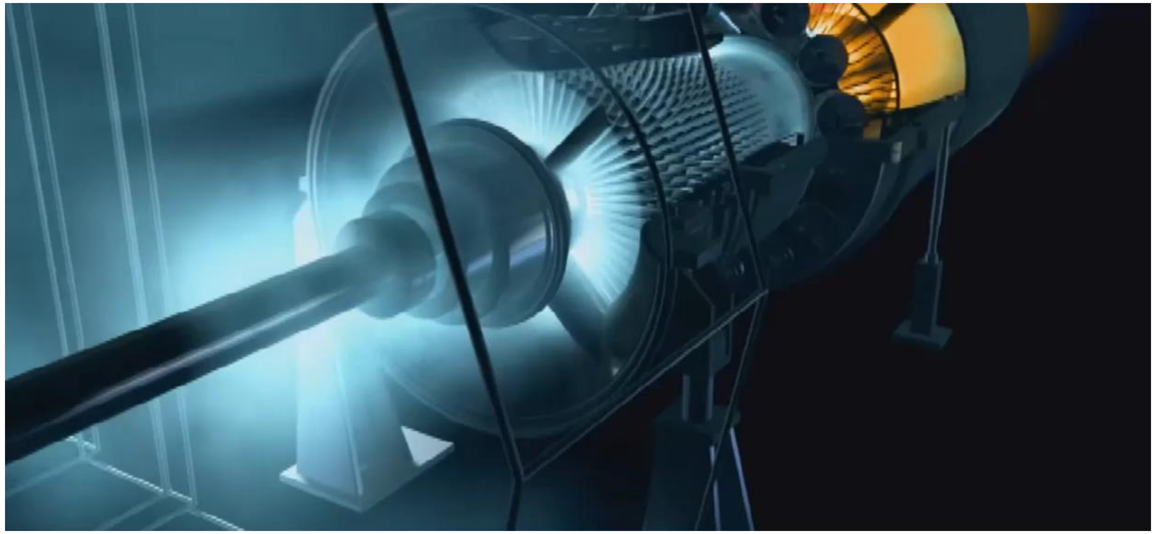

LPBF based Metal AM Process

Image: ANSYS AM Research Lab at Pitt

Project Objective

- Primary goal: To develop a cost-effective quality assurance (QA) method that can rapidly qualify laser powder bed fusion (LPBF) - processed hot gas path turbine components (HGPTCs) through a machine learning framework, which would assimilate in-situ monitoring and measurement, ex-situ characterization, and simulation data.

- Target application: Use the developed QA tool to qualify advanced HGPTC produced by LPBF in Inconel 718.

Task 1 (PI Zhao): Overview of the developed in-situ monitoring system

In-situ Monitoring System
Developed at Pitt's ZIP-AM Laboratory
for Powder Bed Fusion Process (EOS M290)

In-situ Monitoring Subsystem #1:
On-axis Two-wavelength Imaging Pyrometry for Measuring Meltpool Temperature and Morphology

In-situ Monitoring subsystem #2:
Off-axis camera for on-axis data registration and layerwise anomaly detection (powder bed, built part, spatter)

In-situ TWIP for Meltpool Temperature Measurement: Optical calibration

- The optical calibration was done using a visible wavelength neutral density filter.
- The source spectrum was not saturating as can be seen in the plots to the right
- The measurements at output of the optical path were acquired at six different times and averaged for calculating the optical transmission coefficients - A1 and A2 values - at the two wavelength optical paths.
- Based on these experiments, the A1 and A2 ratio was found to be 1.3.

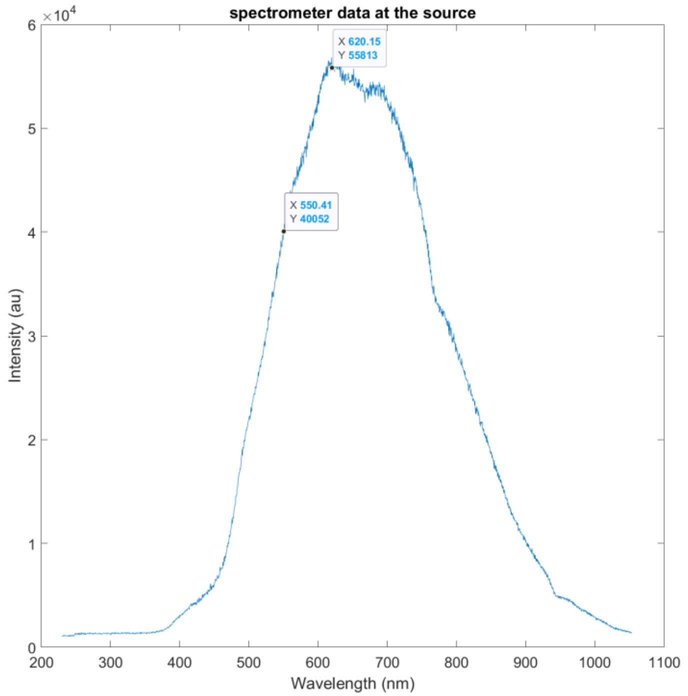

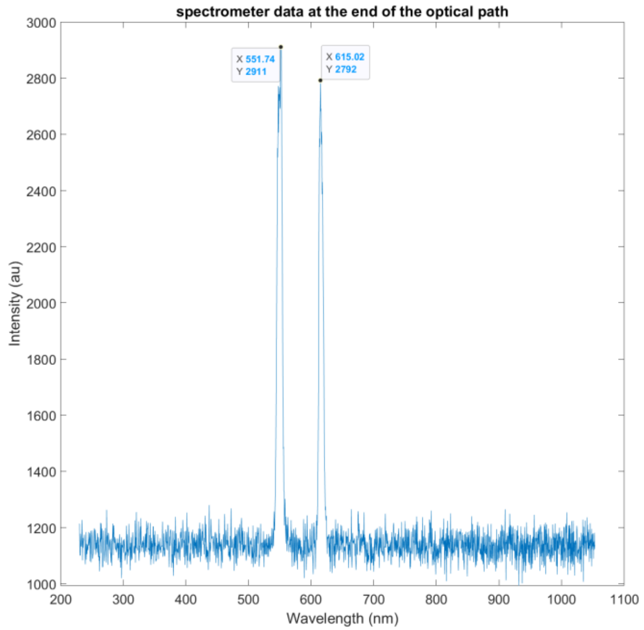

In-situ TWIP for Meltpool Temperature Measurement: Optical calibration

✓ **Optical Calibration was performed to obtain the two-wavelength optics transmission ratio A_1/A_2**

From our experiments, the A1/A2 ratio was determined to be 1.3, which can be plugged into Equation 1 to estimate the meltpool temperature.

$$T = \frac{\frac{hc}{k_B}\left(\frac{1}{\lambda_2} - \frac{1}{\lambda_1}\right)}{\ln R_{12} - 5\ln\left(\frac{\lambda_2}{\lambda_1}\right) - \ln\left(\frac{A_1}{A_2}\right)} \qquad (Eq.1)$$

✓ **Evaluated the Temperature-Intensity curve for our in-situ meltpool monitoring system.**

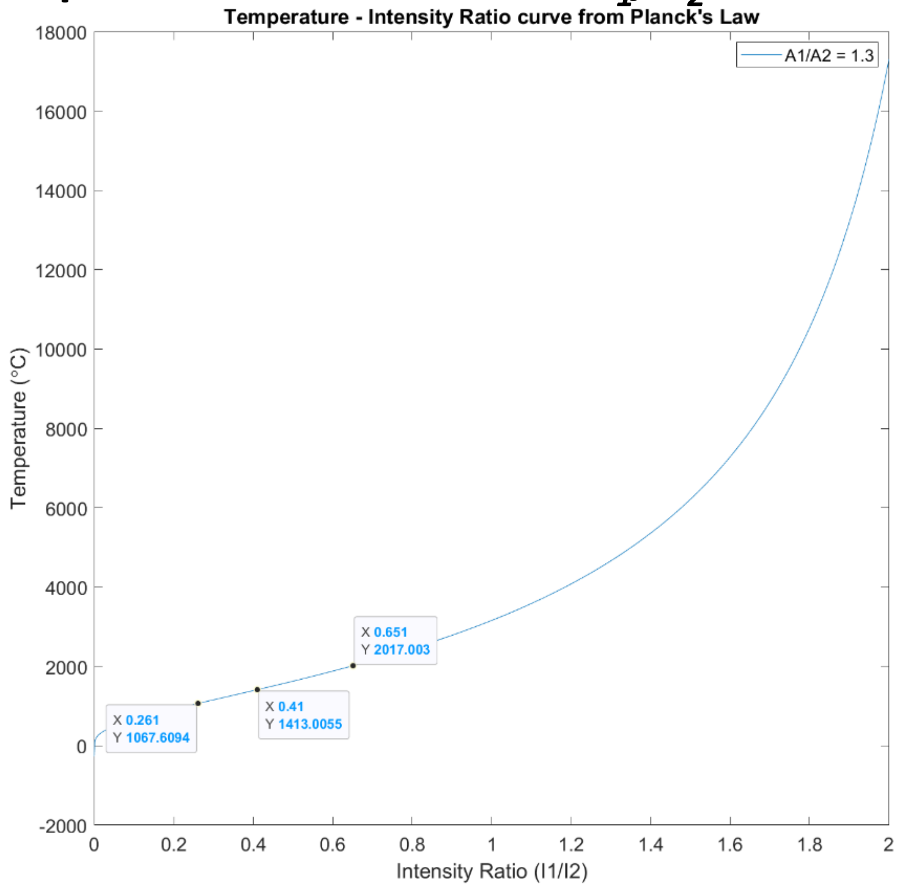

Temperature-Intensity Ratio curve derived from Plank's Law using the A_1/A_2 ratio 1.3

Observation: Rotations and Scaling exist in the two-wavelength images from the same meltpool.

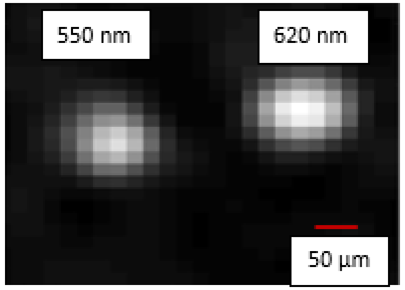

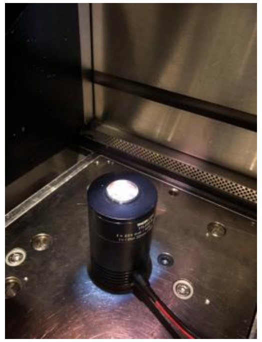

D = 0.5mm

Light source Test (Image of Bulb Filament)

20k fps @256x128

Experimentally,
D1/ D2 = 1.13
620 nm image larger than 550 nm image

Theoretically,

$$w = \left(\frac{4\lambda}{\pi}\right)\left(\frac{f}{d}\right)$$

f---focal length
λ---wavelength
d---incoming beam diameter
w ---focal spot size diameter
Calculated $w1/ w2$ =1.127

Rotation angle between two images = 13 degrees

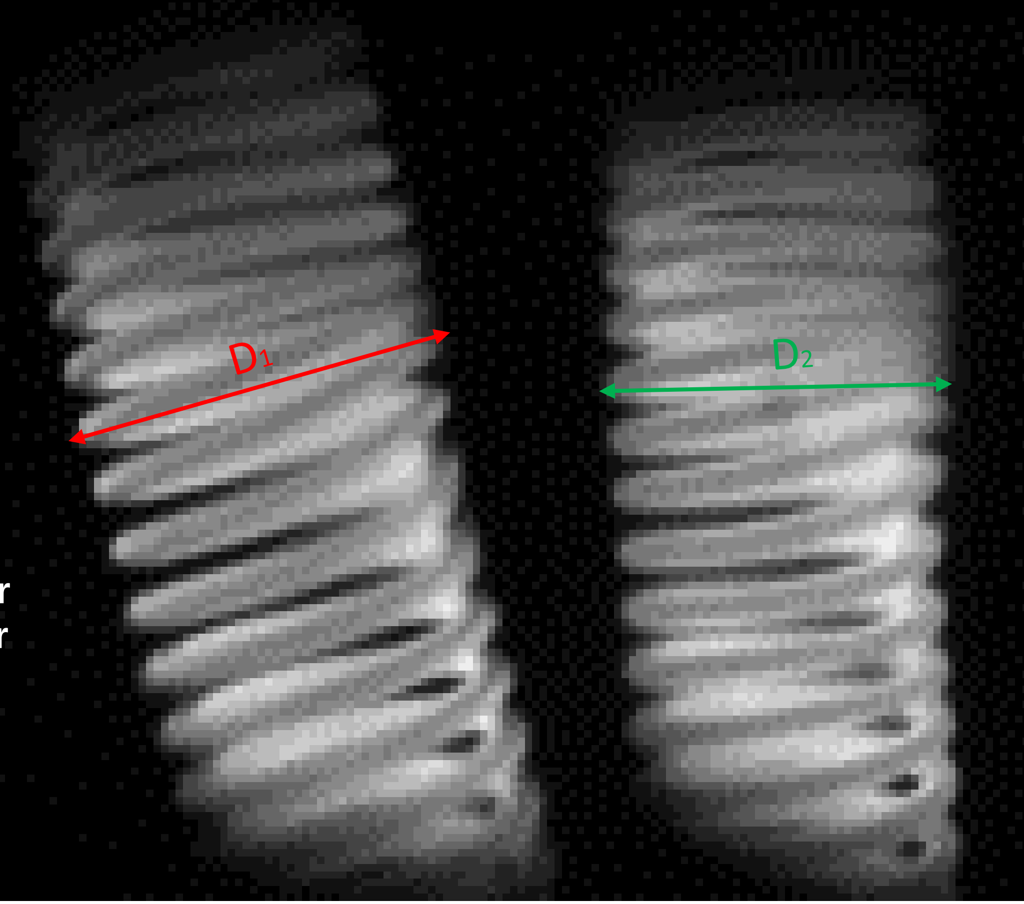

In-situ TWIP for Meltpool Temperature Measurement: Image Processing and Data Analytics

❑ To obtain the two-wavelength intensity ratio which is key to measure the meltpool temperature

Due to the optical losses, the possible minor misalignments in the optical system setup, and chromatic aberrations, it was observed that the acquired meltpool image data for two wavelengths are not exactly the same (in alignment and size).

Our Approach: implement a feature recognition algorithm, known as the KAZE algorithm to obtain the scaling and rotation between the two-wavelength meltpools. An example of the result for such transformation is illustrated in Fig A. These transformed images are further used for obtaining their intensity ratio (Fig B). This intensity ratio will be substituted in Plank's law for obtaining the temperature distribution in the meltpool

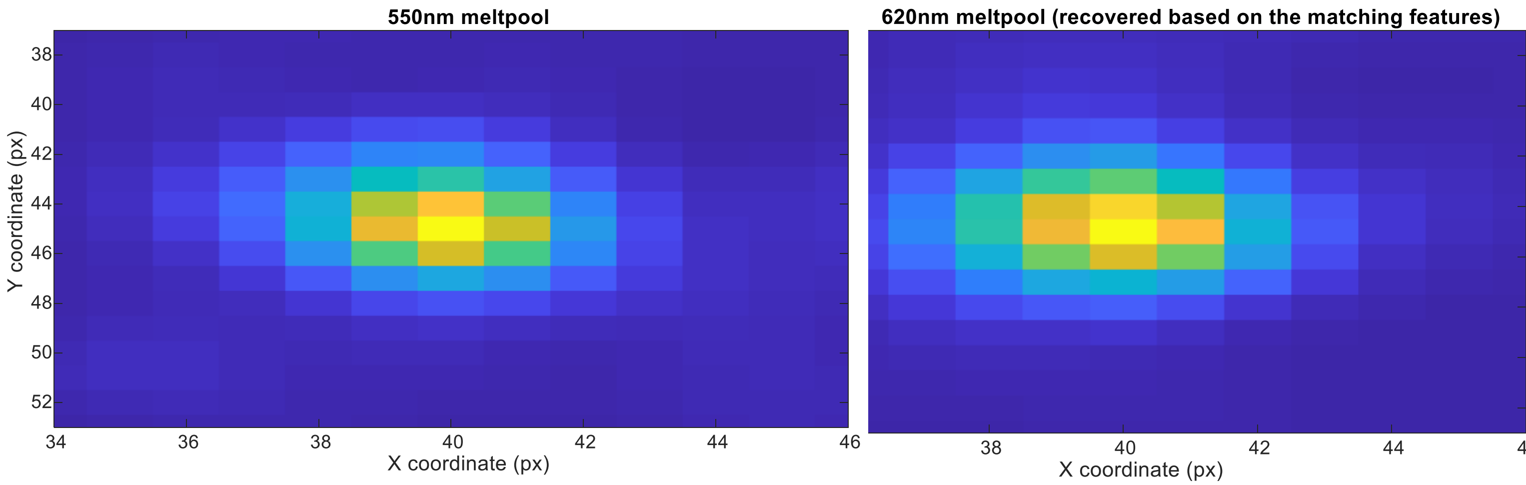

In-situ TWIP for Meltpool Temperature Measurement: Validating with Thermocouple

- **To validate the temperature measurement**, Thermocouple measurements of the meltpool need to be acquired independently. To realize this, initial set of experiments were performed with some success in terms of recording the actual temperatures values. Further experiments will be performed to complete this validation step, these experiments will be completed before the end of this quarter (12/2020).

Videos of TWIP Validation Experiment:

(Left) LPBF AM process. The experiments were performed with a laser power of 200 W and scan speed of 50mm/s.

(Right) In-situ TWIP sensor data. Each frame consists of two wavelength images of a meltpool.

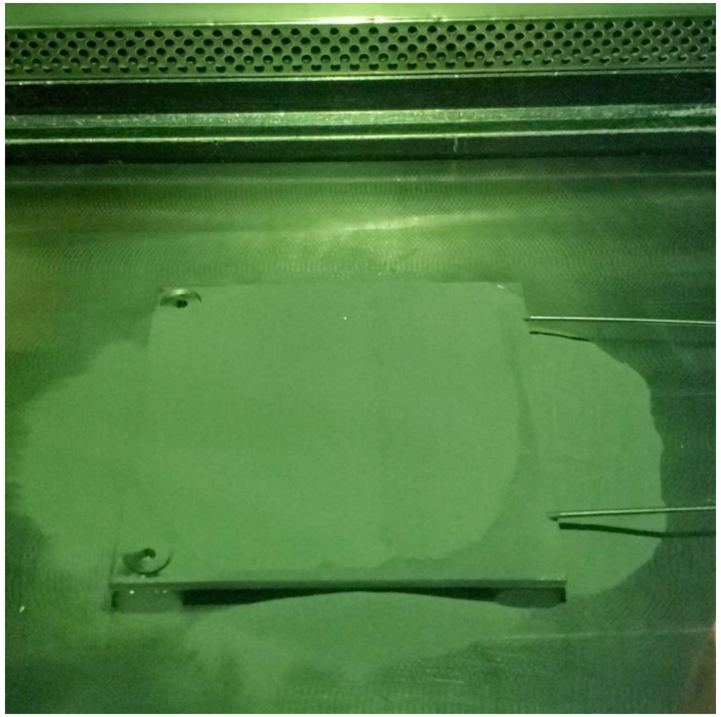

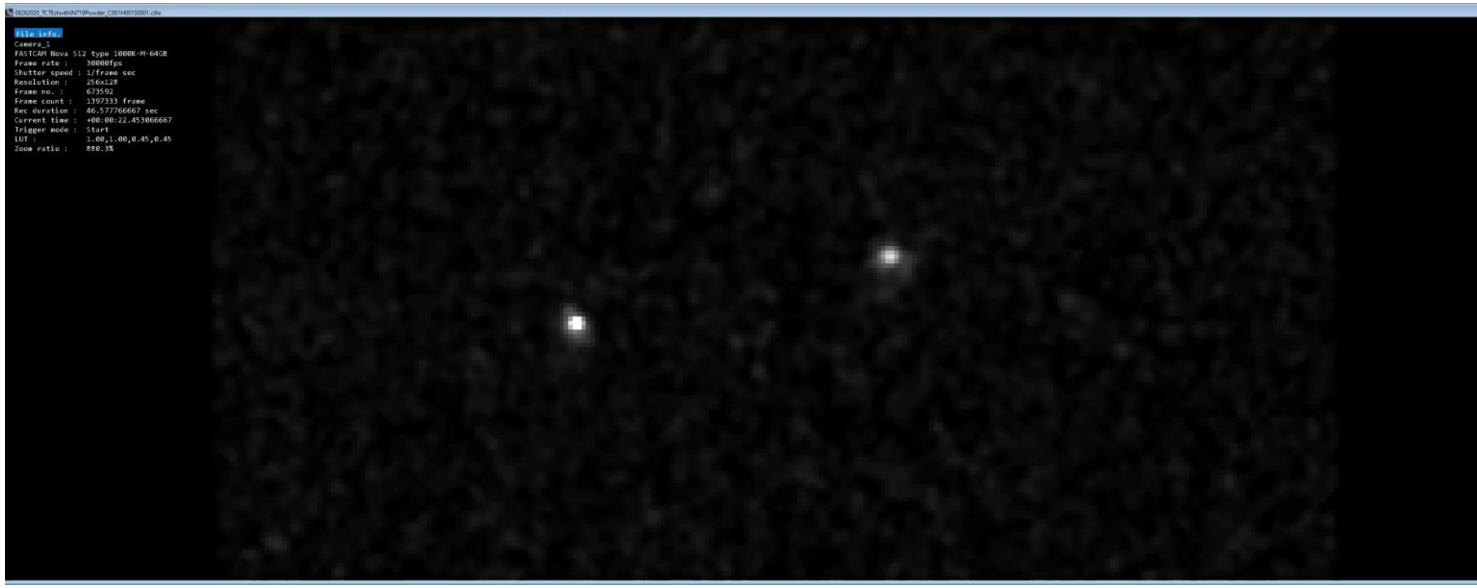

In-situ TWIP for More Meltpool Properties such as Morphology

In addition to Meltpool Temperature Measurement, the developed TWIP is also capable of monitoring and measuring Meltpool Morphology (e.g., area, width, ellipticity).

- Developed a code for estimating the area of the meltpool by fitting an ellipse to the boundary of the meltpool.
- The ellipse parameters in pixels are estimated from the code, which can be converted to microns using the pixel resolution.
- The code can be applied to multiple frames simultaneously and the area can be estimated for both the meltpools.
- The ellipse parameters are estimated based on a curve fit
- The semi axes lengths and the centers are determined based on these equations
- Area of the ellipse is given by π×a’×b’

Ellipse fit to the boundary of the meltpool

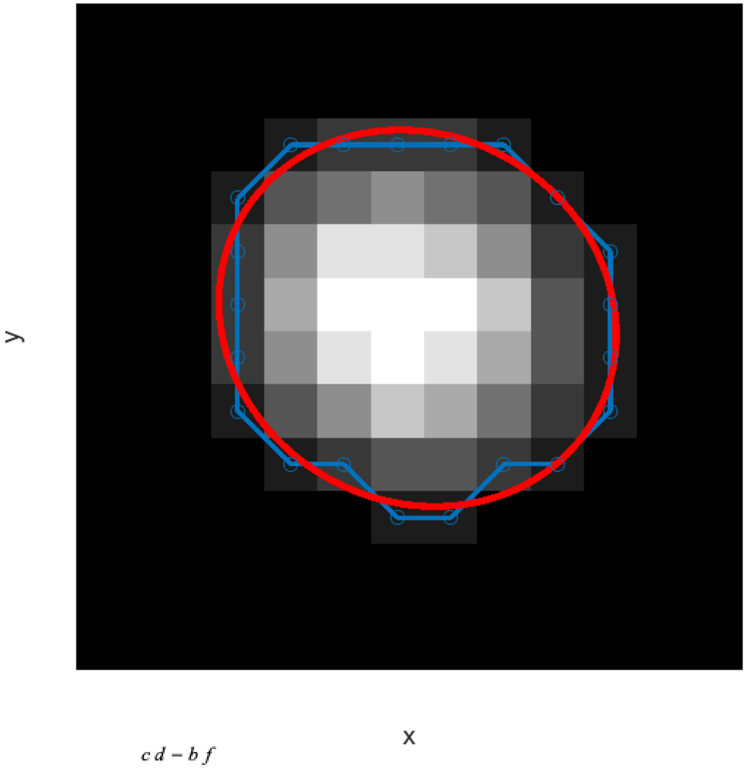

$$x_0 = \frac{c\,d - b\,f}{b^2 - a\,c}$$

$$y_0 = \frac{a\,f - b\,d}{b^2 - a\,c},$$

the semi-axis lengths are

$$a' = \sqrt{\frac{2\left(a\,f^2 + c\,d^2 + g\,b^2 - 2\,b\,d\,f - a\,c\,g\right)}{\left(b^2 - a\,c\right)\left[\sqrt{(a-c)^2 + 4\,b^2} - (a+c)\right]}}$$

$$b' = \sqrt{\frac{2\left(a\,f^2 + c\,d^2 + g\,b^2 - 2\,b\,d\,f - a\,c\,g\right)}{\left(b^2 - a\,c\right)\left[-\sqrt{(a-c)^2 + 4\,b^2} - (a+c)\right]}}.$$

Experiment with In-situ TWIP: To Evaluate the Meltpool Monitoring Capabilities

Three sets of experiment were conducted.

- **Experiment Set #1: Single track experiments on bare IN718 plates for different processing conditions**
  In-situ meltpool monitoring data was acquired for a period of 2.5 seconds at 75,000 fps
- **Experiment Set #2: Single track experiments on bare IN718 plates for different processing conditions**
  In-situ meltpool monitoring data was acquired for a period of 2.5 seconds at 50,000 fps
- **Experiment Set #3: A complete build of five fatigue bar samples designed per ASTM standards**
  The fatigue bar print consisted of 95 layers, out of which 20 layers of data was acquired.

Table: Three different frame rates for evaluating the minimum frame rate requirement for meltpool monitoring

Layer Print Time (s)	Meltpool Data Acquisition Rate (fps)	Number of Meltpool Frames for each printed layer
70	40,000	2.8 million
70	18,000	1.26 million
70	10,000	0.7 million

The frame number and data volume should be multiplied by the number of layers. The overall data size can be even larger with bigger parts.

Require high-performance computing to analyze these big monitoring data for meltpool signatures (e.g., intensity, area, width, and temperature).

Experiment with In-situ TWIP: To Evaluate the Meltpool Monitoring Capabilities

- **Experiment Set #1: Single track experiments on bare IN718 plates for different processing conditions**
  In-situ meltpool monitoring data was acquired for a period of 2.5 seconds at **75,000 fps**

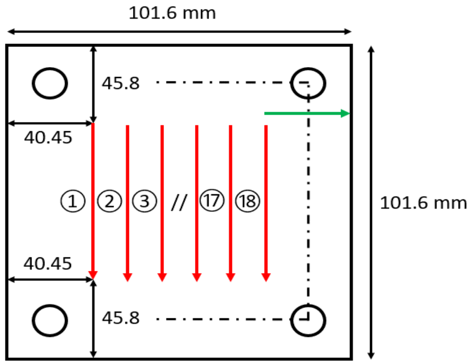

Build Plate 1: Preheat Temperature = 80 °C, Layer Thickness = 40 um					
Track Number	Power (W)	Velocity (m/s)	Preheat temp. (°C)	Layer thickness (um)	Power Density (J/m)
1	100	0.50	80	40	200.00
2	100	1.00	80	40	100.00
3	100	1.50	80	40	66.67
4	150	0.50	80	40	300.00
5	150	1.00	80	40	150.00
6	150	1.50	80	40	100.00
7	200	0.50	80	40	400.00
8	200	1.00	80	40	200.00
9	200	1.50	80	40	133.33
10	250	0.50	80	40	500.00
11	250	1.00	80	40	250.00
12	250	1.50	80	40	166.67
13	285	0.50	80	40	570.00
14	285	1.00	80	40	285.00
15	285	1.50	80	40	190.00
16	350	0.50	80	40	700.00
17	350	1.00	80	40	350.00
18	350	1.50	80	40	233.33
19	225	1.25	80	40	180.00
20	325	1.00	80	40	325.00

Experimental schematic for single-track experiments on bare IN718 plates along with the processing conditions for each single-track

Machine learning of the process conditions, meltpool signatures, and part properties will be performed.

Figures: Variation of Meltpool Area (Top) and Meltpool Width (Bottom) Note: The spike in the data correspond to laser turn off times.

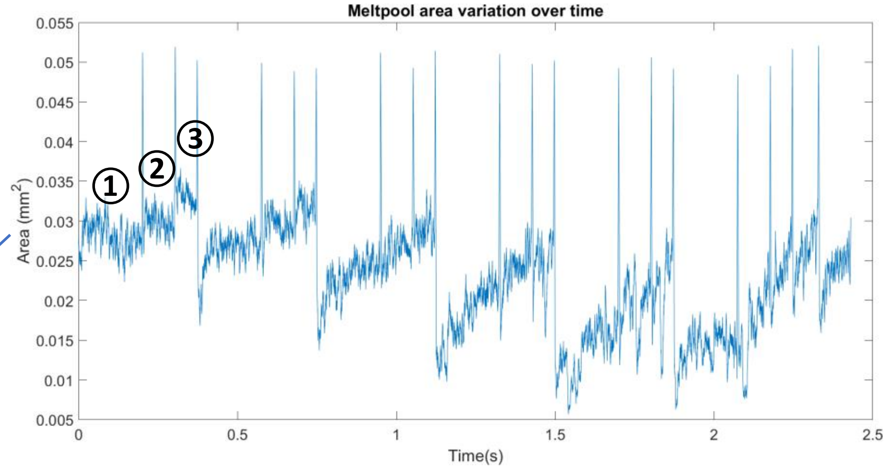

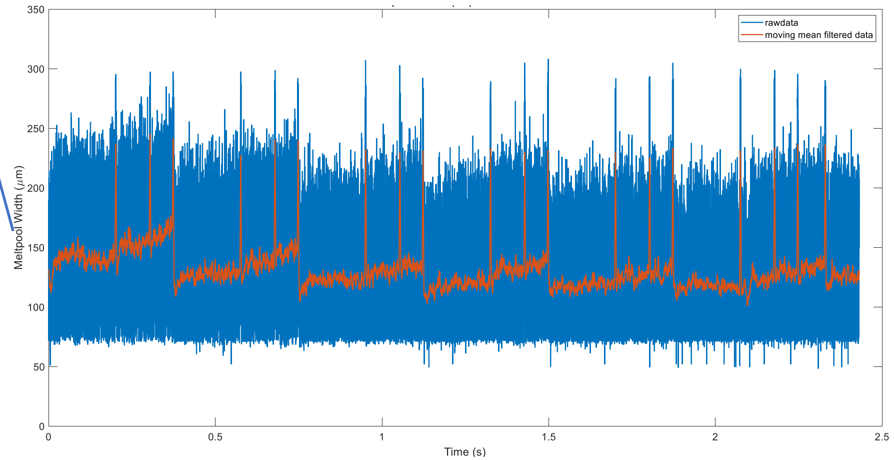

Experiment with In-situ TWIP: To Evaluate the Meltpool Monitoring Capabilities

- **Experiment Set #3: A complete build of five fatigue bar samples designed per ASTM standards**

  The fatigue bar print consisted of 95 layers, out of which 20 layers of data was acquired.

  Apart from the in-situ monitoring, X-Ray CT tests and other mechanical testing (such fatigue testing) will be performed on the printed samples by Co-PI Neu's team at GaTech. The X-Ray CT data will then be compared with the in-situ monitoring data for any signatures indicating defects or anomalies.

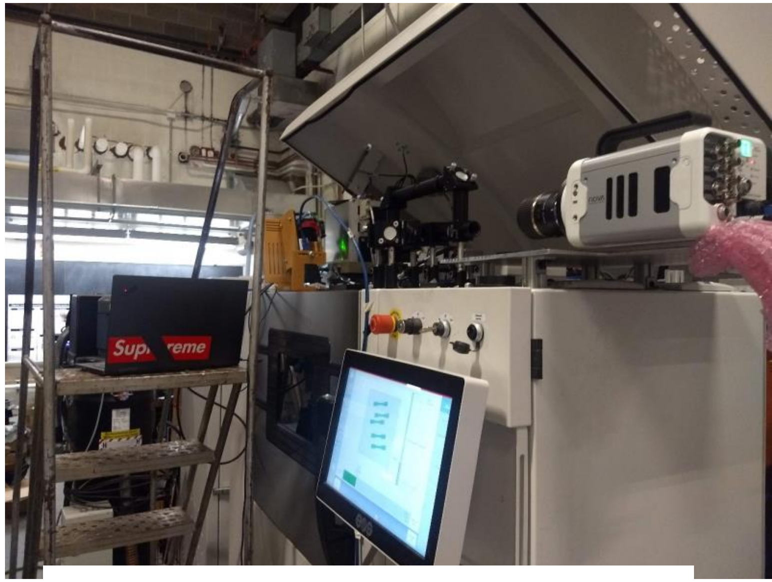

Experimental setup for MP data acquisition

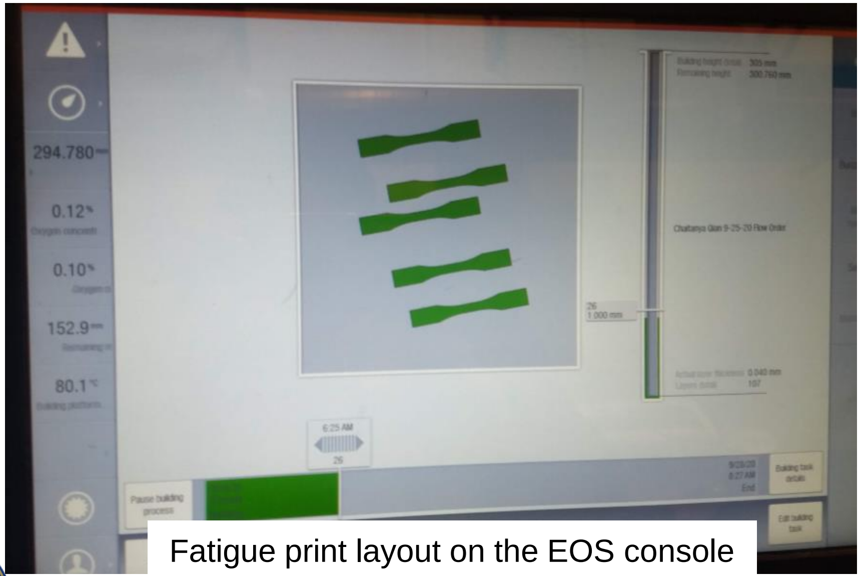

Fatigue print layout on the EOS console

Snapshot of the fatigue bar print

Printed fatigue bar samples (numbered)

Experiment with In-situ TWIP: To Evaluate the Meltpool Monitoring Capabilities

- **<u>Data Acquisition and Storage</u>**: An example in-situ meltpool monitoring video is shown below. Each fatigue bar print time is approximately 14.4 secs and each fatigue bar print is separated by 0.3s, which can be clearly seen in the monitoring video. Each printed layer's video data is divided into five segments of each fatigue bar's meltpool image data. *The data transfer took longer than expected (>16 hours for a file over LAN) due to the large data files and some network issues*.
- **<u>Data Processing and Analytics</u>**: The data processing is in progress. From the intensity monitoring of each layer, we will extract all the key features including each meltpool's temperature profile, size, shape, and location, as well as hatching pattern for each print layer.

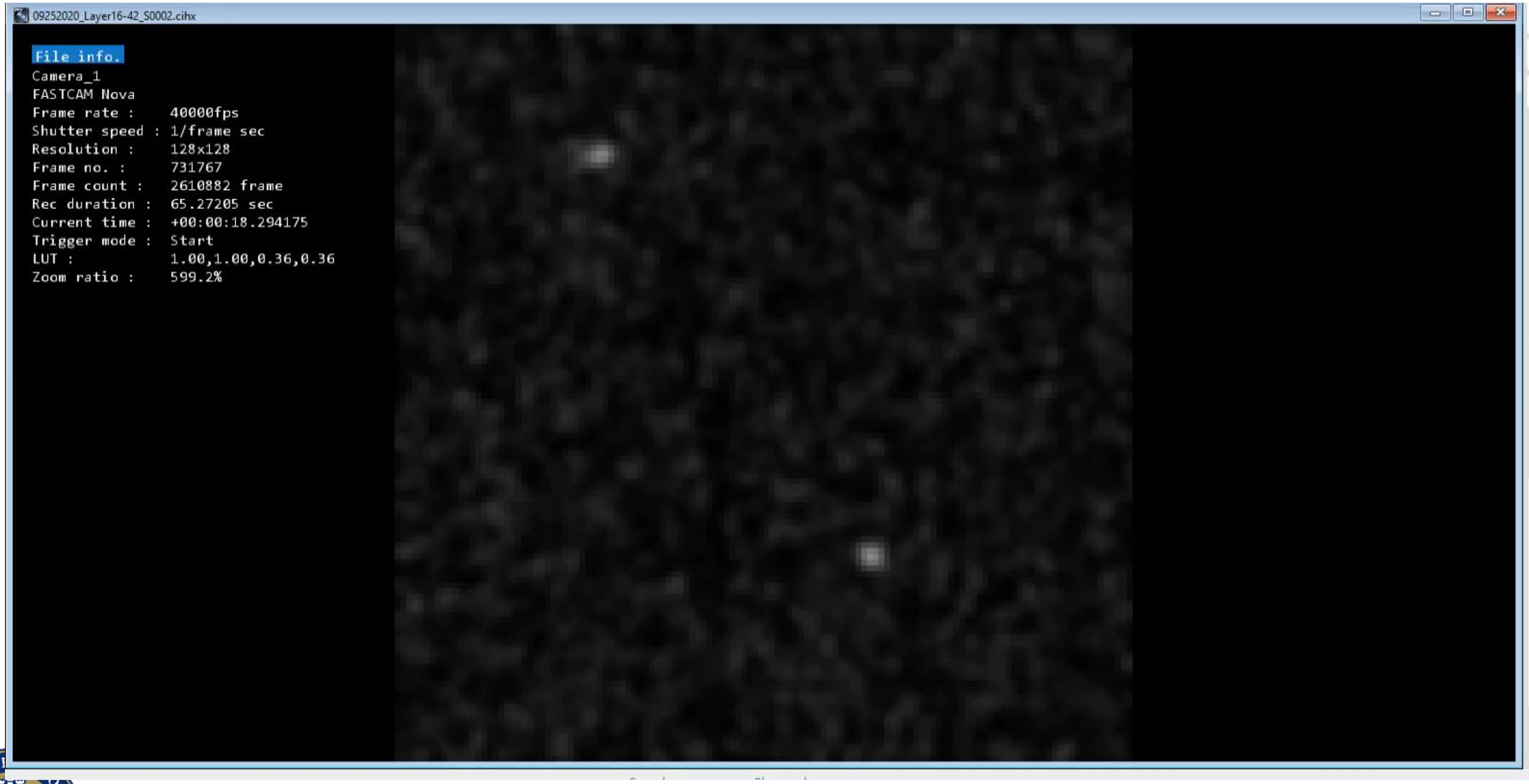

Labeled fatigue bar samples printed on 09/25. These samples were shipped to GaTech for characterization and testing

In-situ TWIP: Improved Optical Design by using a Beam Expander

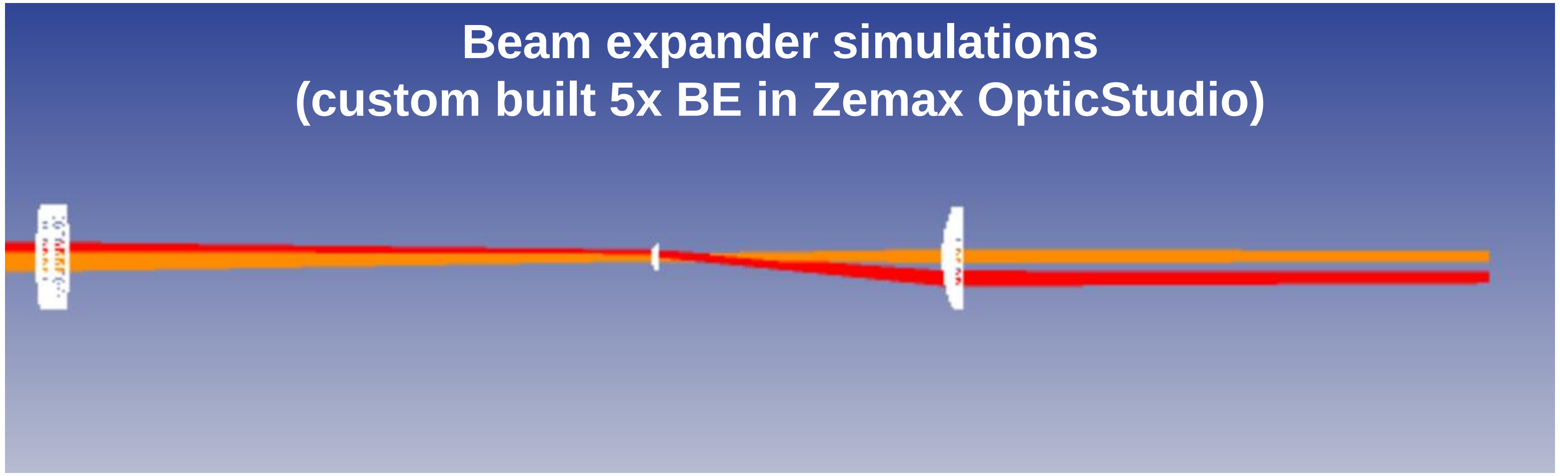

Optical simulation of two beams (550nm and 620nm)
(Left) with and (Right) without a beam expander

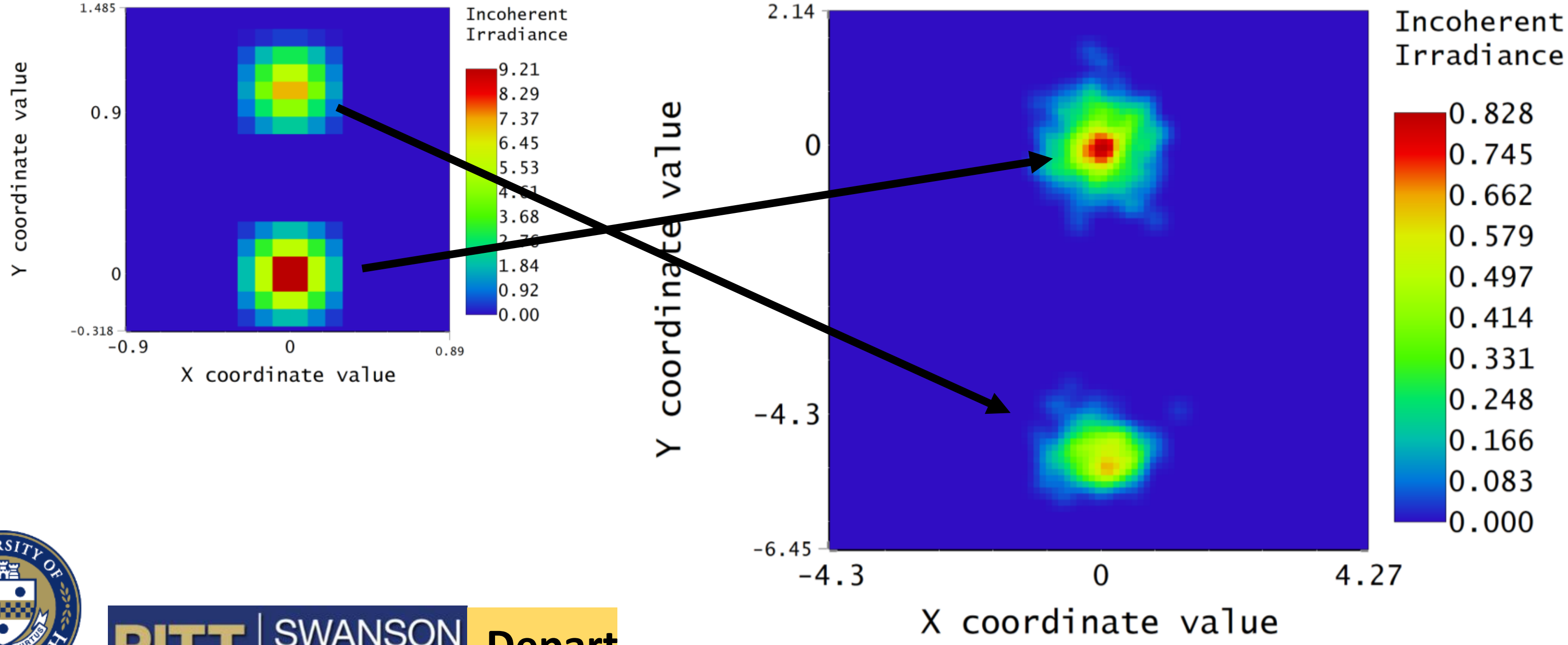

<u>Observation:</u>

- **Spatial resolution of the meltpool is improved**
- **BE can help further reduce chromatic aberrations.**
- **But, there could be a depreciation in the radiance (intensity) of the laser beams.**

In-situ Monitoring with an Off-axis Camera for Layer Monitoring

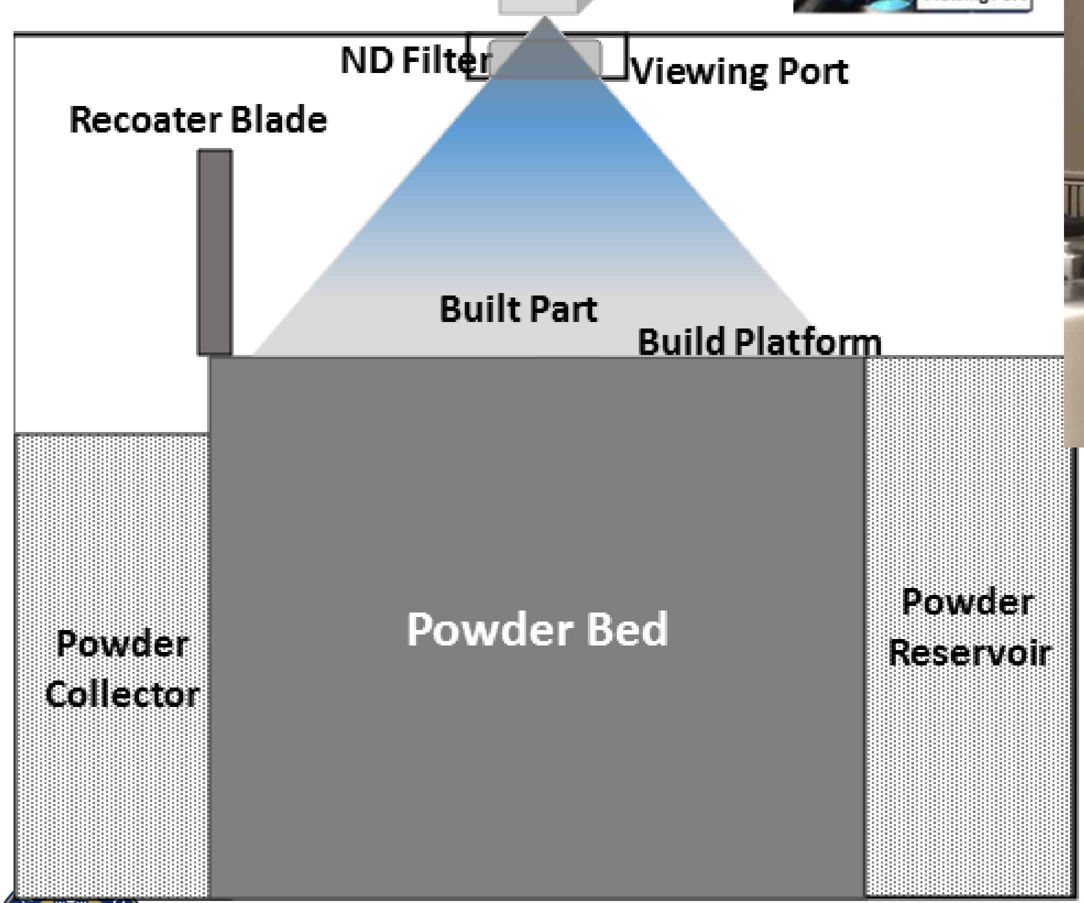

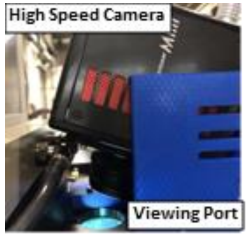

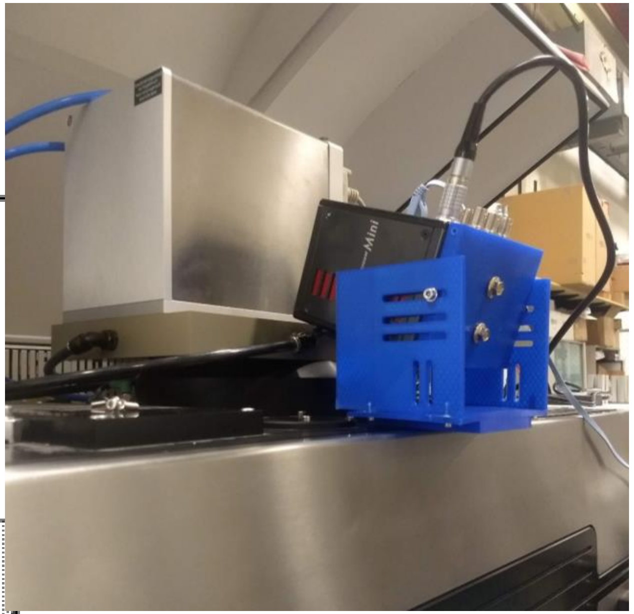

Representative print-layer data Recorded at 500 fps, playback speed 40 fps

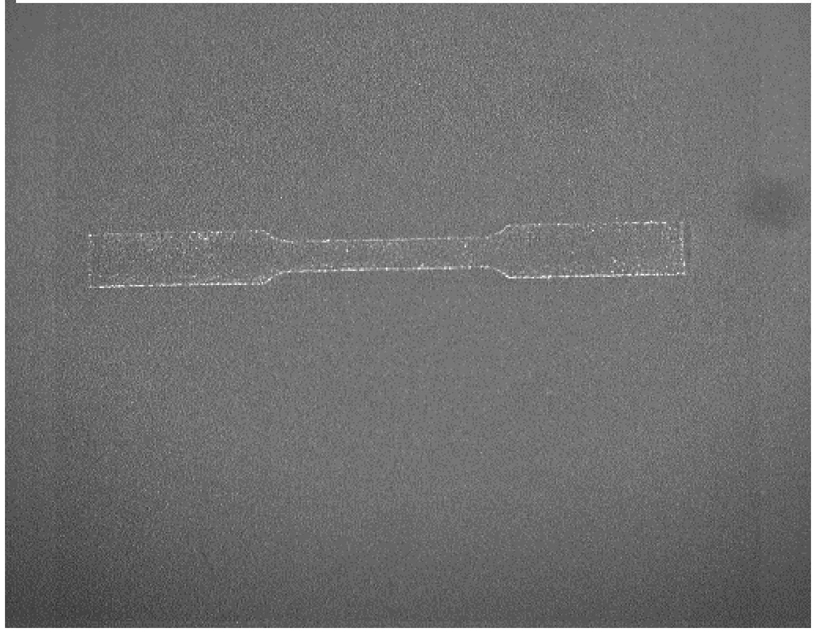

- A high-speed camera was utilized for off-axis in-situ monitoring of a LPBF print
- Videos recorded at 500 fps for 98 layers of the print
- Both image and video data from each layer is extracted for analysis

In-situ Off-axis Camera: Anomaly Detection based on image intensity profile

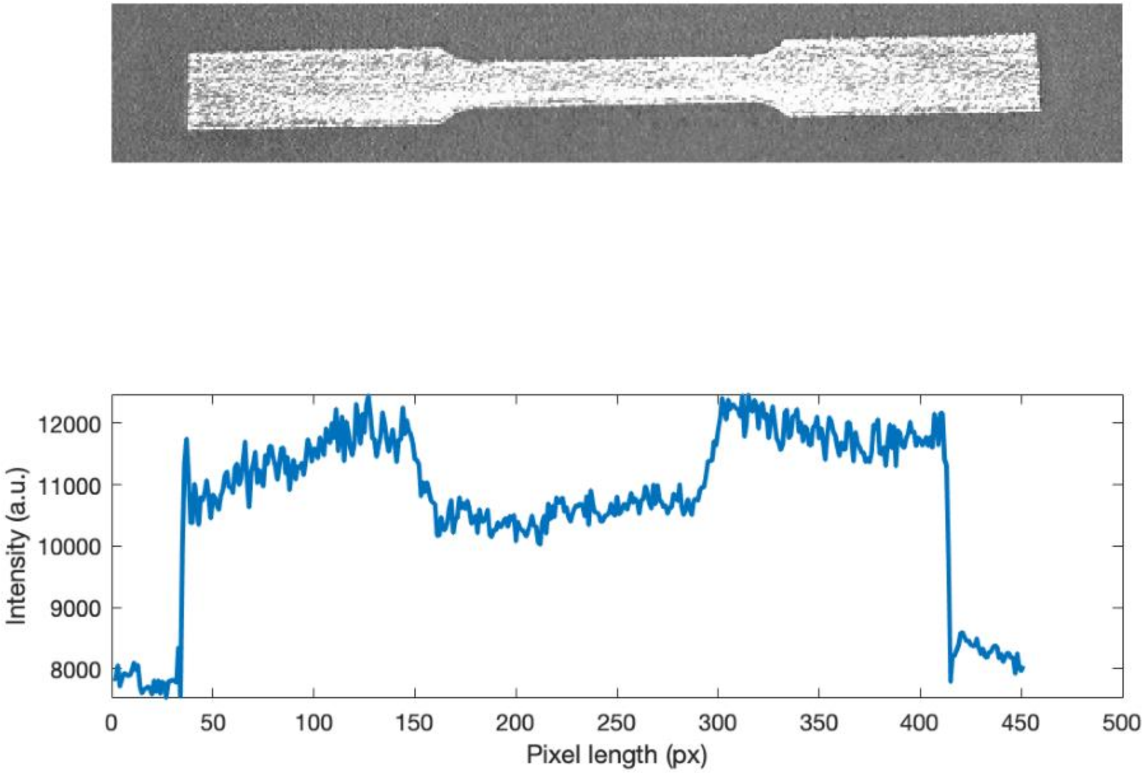

Ideal layer, with no observed flaws. The intensity profile for this layer serves as the benchmark for identifying flaws through the intensity profile

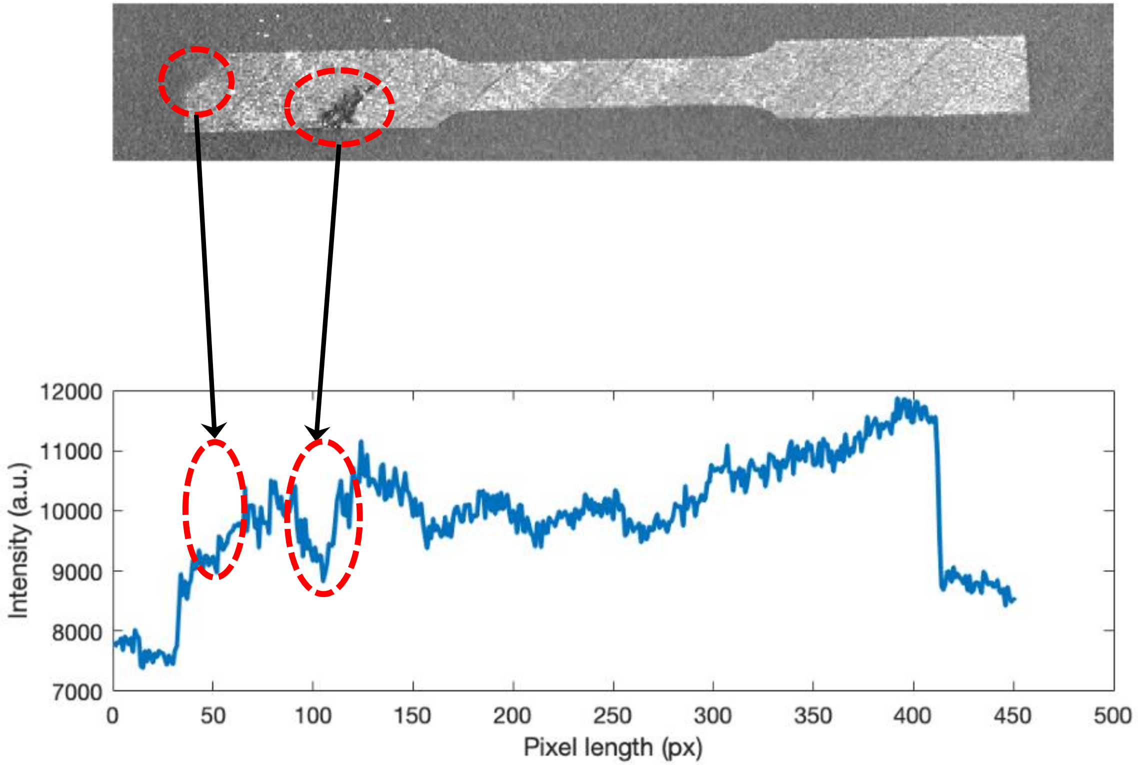

Print layer with some flaws, the observed flaws reflect in the intensity of the layer as shown.

In-situ Off-axis Camera: Deep Learning for Anomaly Classification

- Developed a Convolutional Neural Network based on existing architectures
- Validated the architecture by introducing “flaws” of different pixel size
- Flaws occurred during the print were also successfully identified and classified as “small”/”big” flaws based on their size

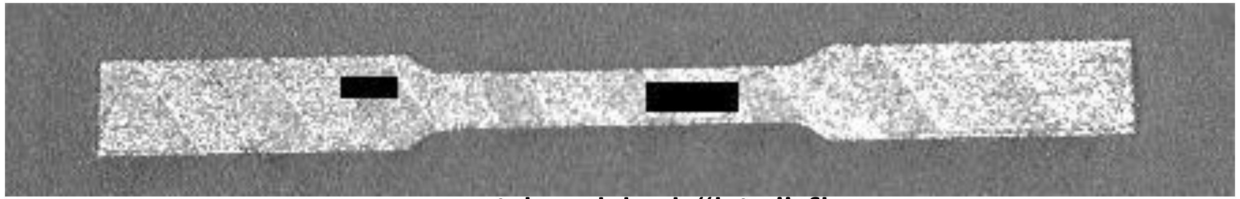

Image with added “big” flaws

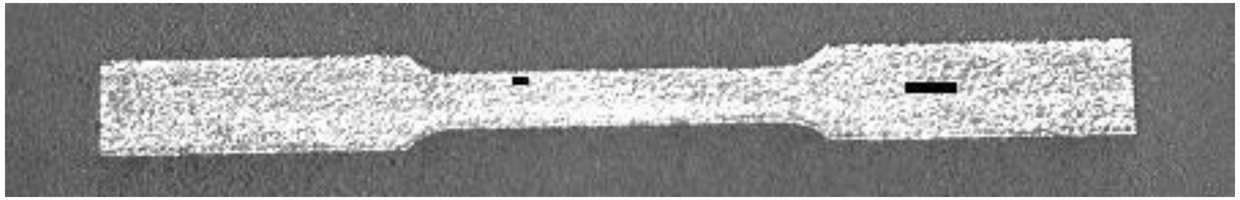

Image with added “small” flaws

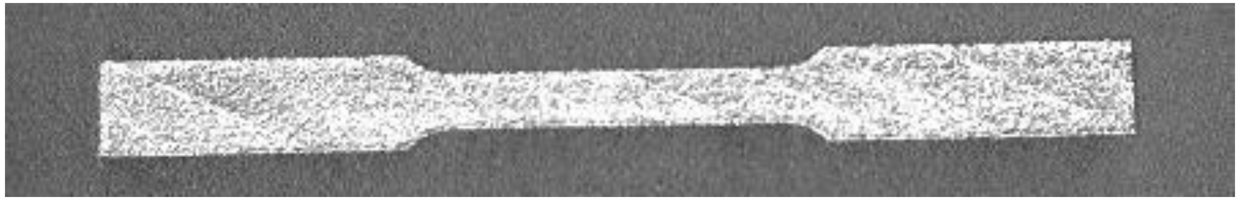

Image with no flaws

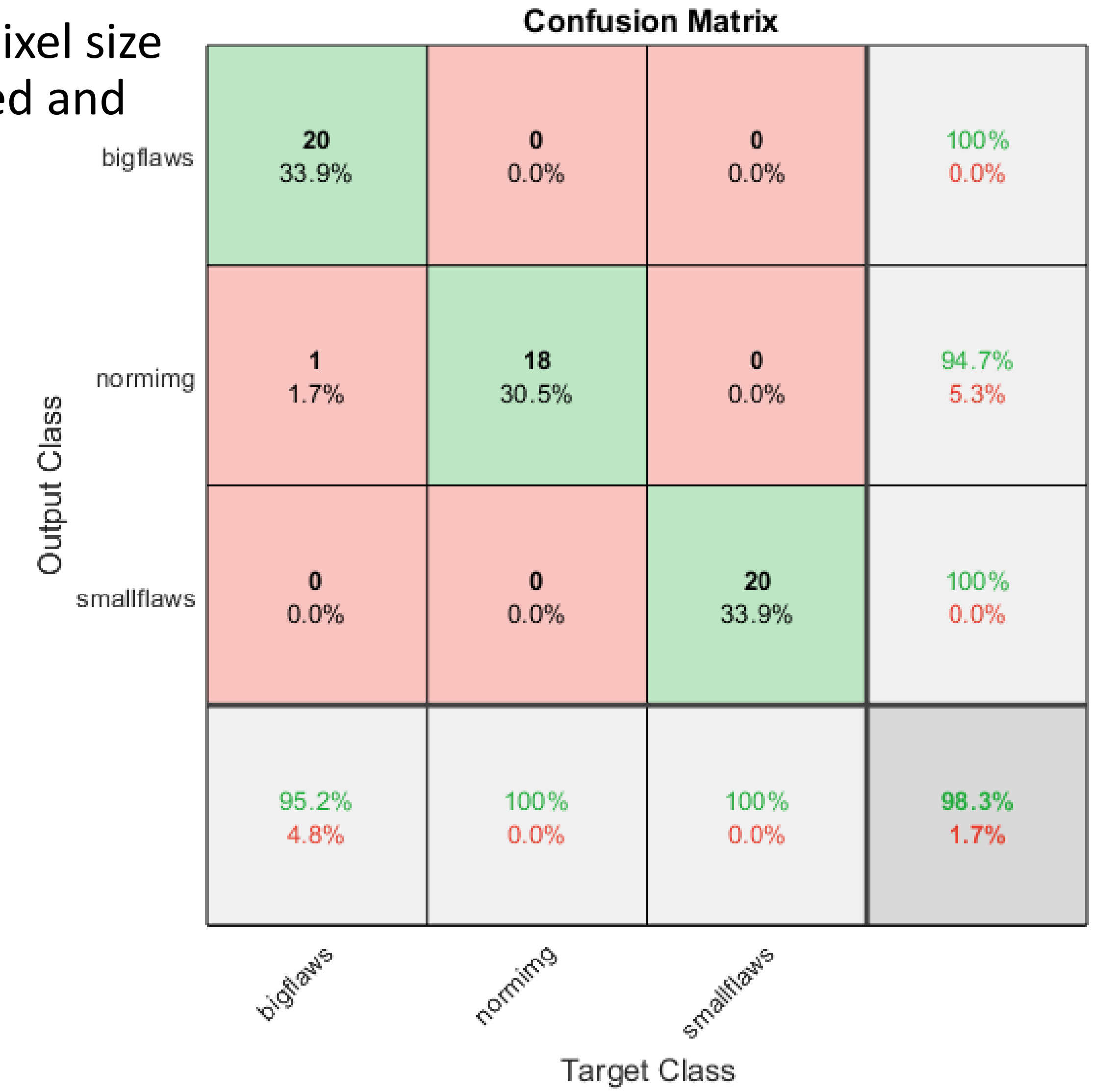

In-situ Off-axis Camera: Spatter detection from layer wise print data

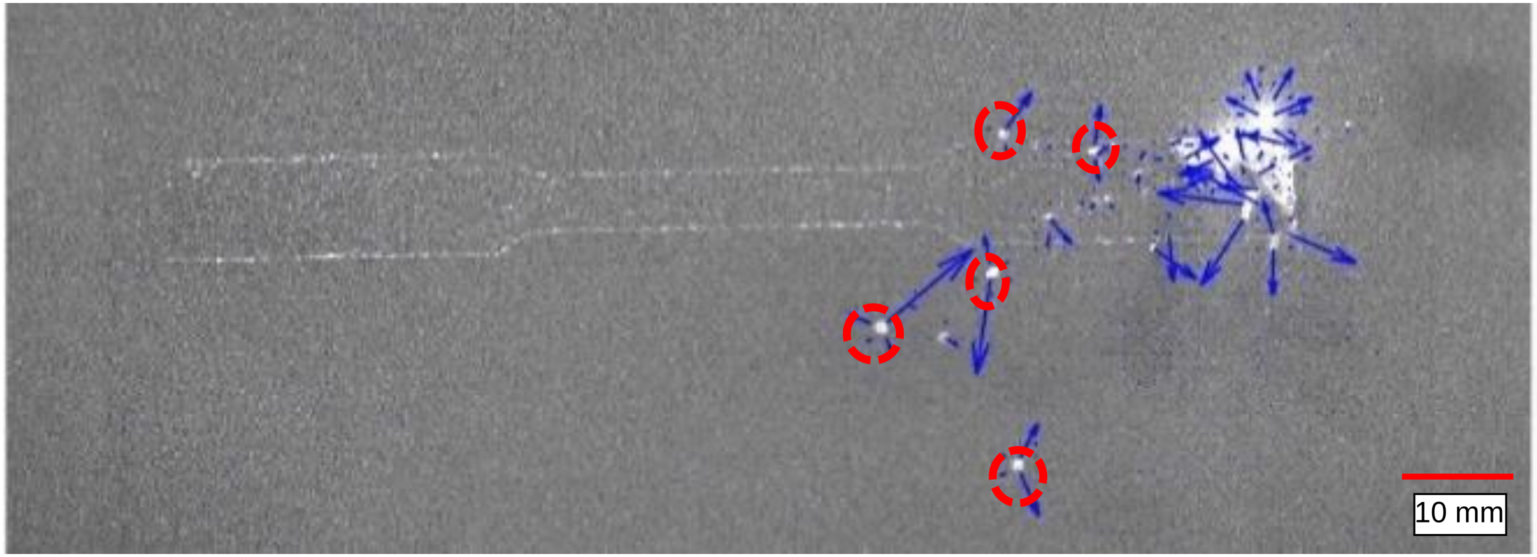

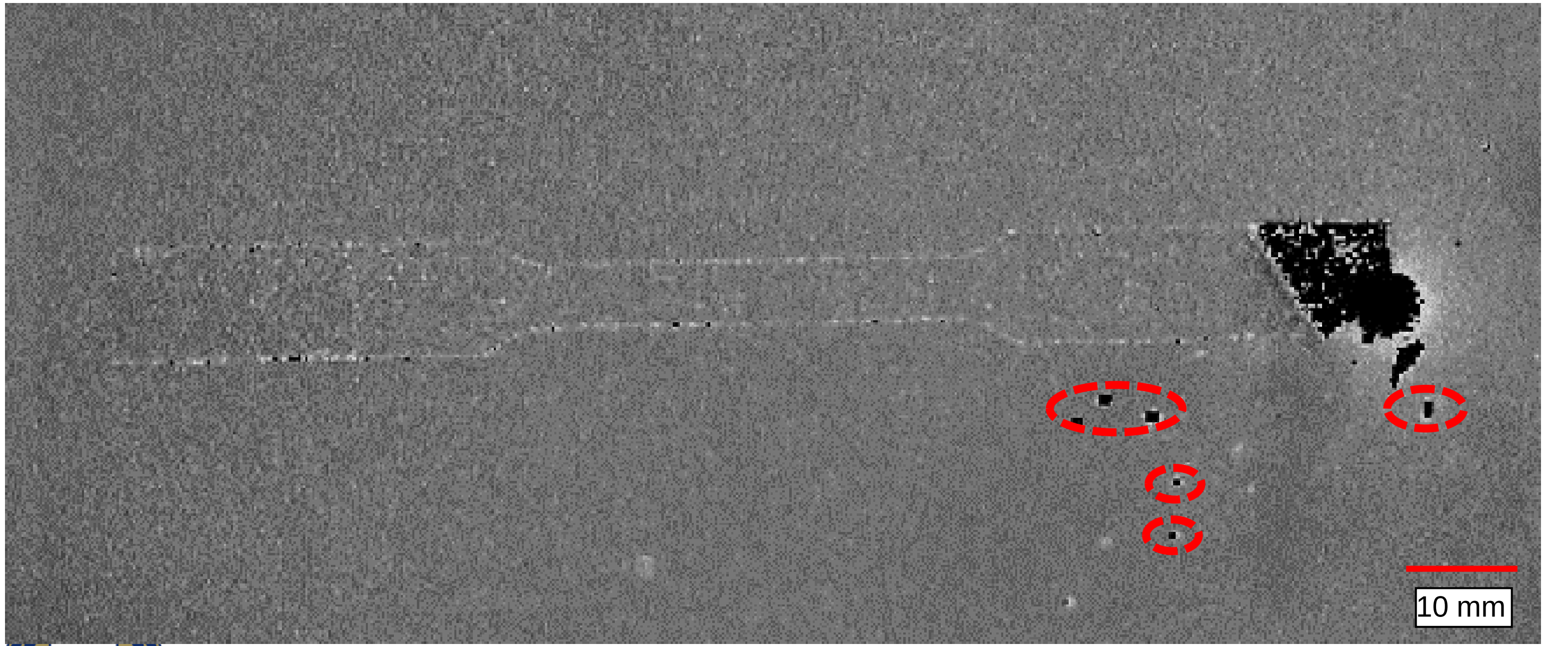

- Spatter analysis was performed using Computer Vision algorithms
- Spatter travel and landing locations can be identified using this method
- Helpful tool to study spatter dynamics and will be further developed to study how spatter effects the neighboring parts and consequent layers

Integrated In-situ Monitoring
Off-axis Camera Synchronized with the On-axis TWIP Camera

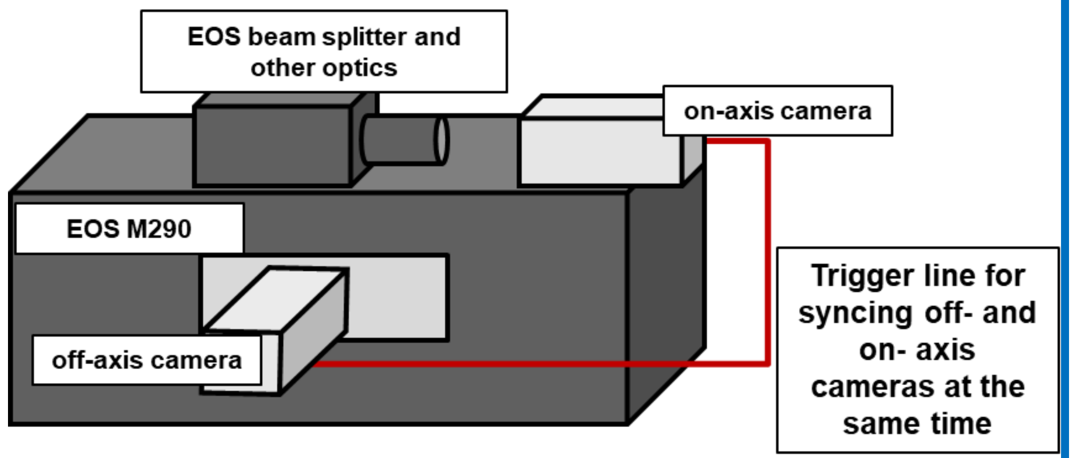

Schematic showing the off- and on- axis camera setup

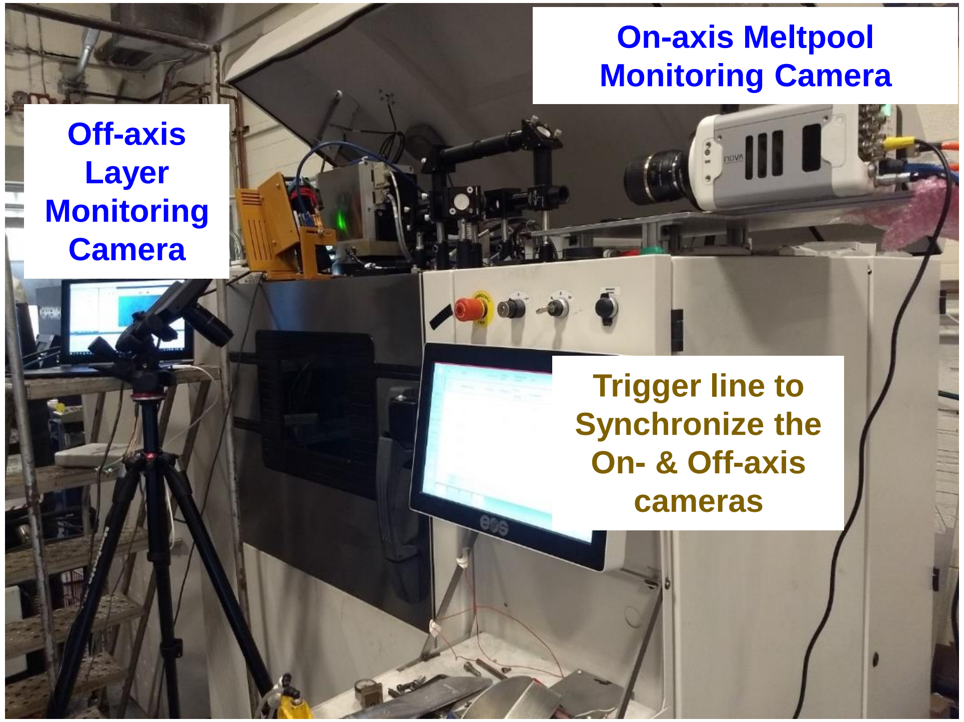

DAQ specifications:

- Frame rate – 1000 fps
- Shutter speed – 500 us
- Resolution – 2560 * 2048
- Pre-processing – (for improving the SNR, increasing the frame rates, good for low light setting and reducing the data size)

Key Outcome: Achieved an Integrated in-situ Monitoring for LPBF AM

Video: Synchronized On-axis Meltpool and Off-axis Layer Monitoring

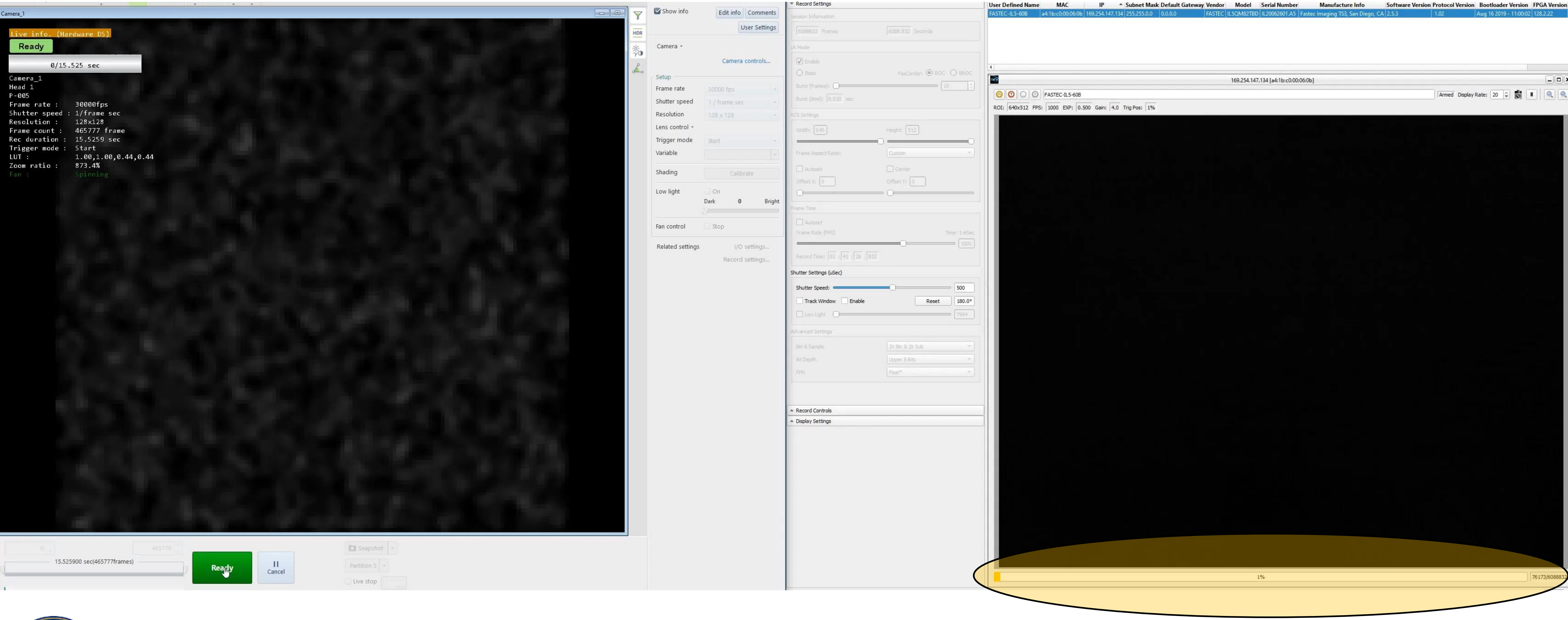

Outline

- Experimental Setup & Results
- Multiphysics Model Calibration
- Key Findings & Discussions:
  - *Temperature dependent material properties*
  - *Evaporation mass*
  - *Laser drill rate*
  - *Scan track length variation*
- P-V and Preheating Process Map

Qian Chen, Yunhao Zhao, Seth Strayer, Yufan Zhao, Kenta Aoyagi, Yuichiro Koizumi, Akihiko Chiba, Wei Xiong, Albert To. Elucidating the effect of preheating temperature on melt pool morphology variation in Inconel 718 laser powder bed fusion via simulation and experiment. ***Additive Manufacturing (Accepted)***

Experiment Setup

Single track depositions on bare plate heated up to different temperature:

- Preheating temperature is: 100 °C, 200 °C, 300 °C, 400 °C and 500 °C;
- The laser power is: 200 W, 250 W, 285 W and 350 W;
- The scan speed is: 0.5 m/s, 0.75 m/s, 1 m/s and 1.5 m/s;
- Single tracks are cross-sectioned in the middle by electrical discharge machine;
- After polishing and etching, the specimens are measured optically by ZEISS Smart Zoom.

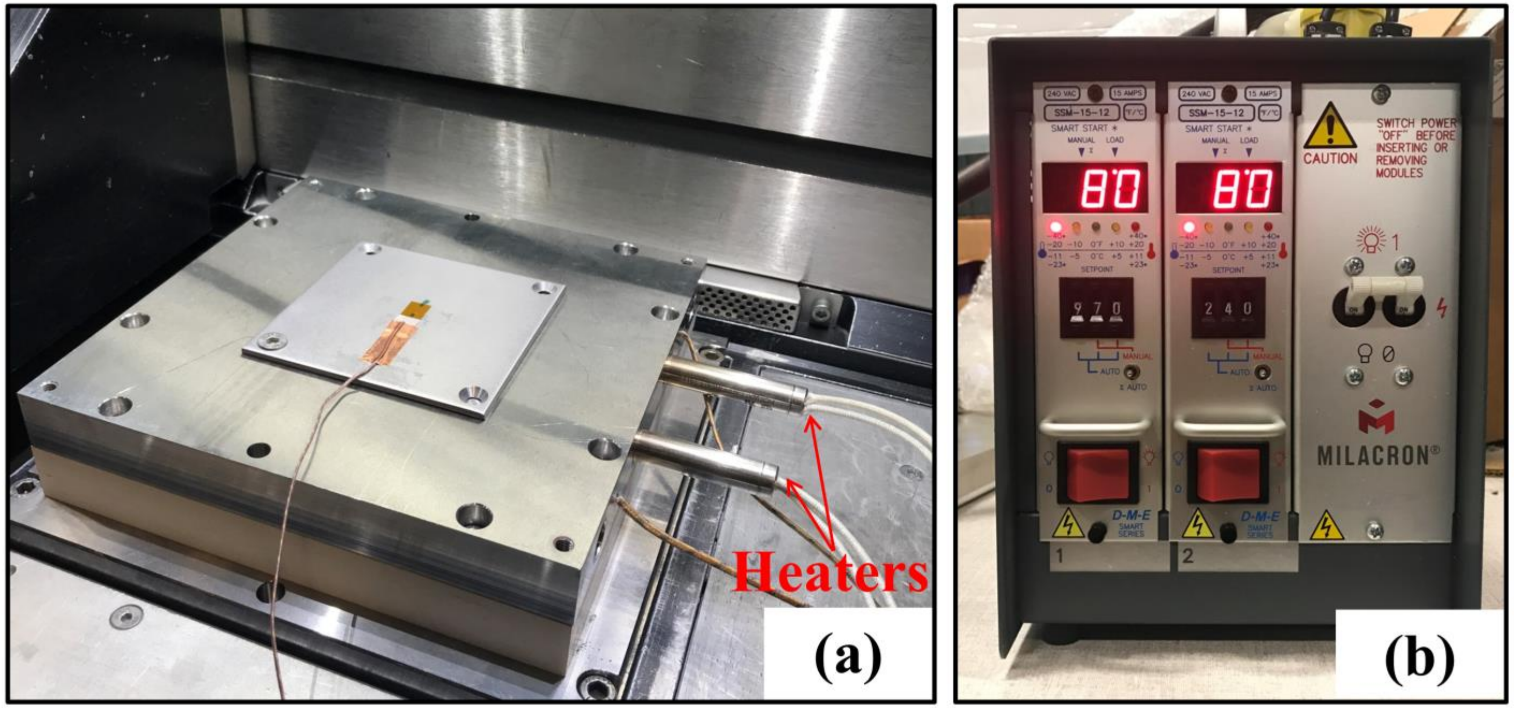

Experimental Measurements

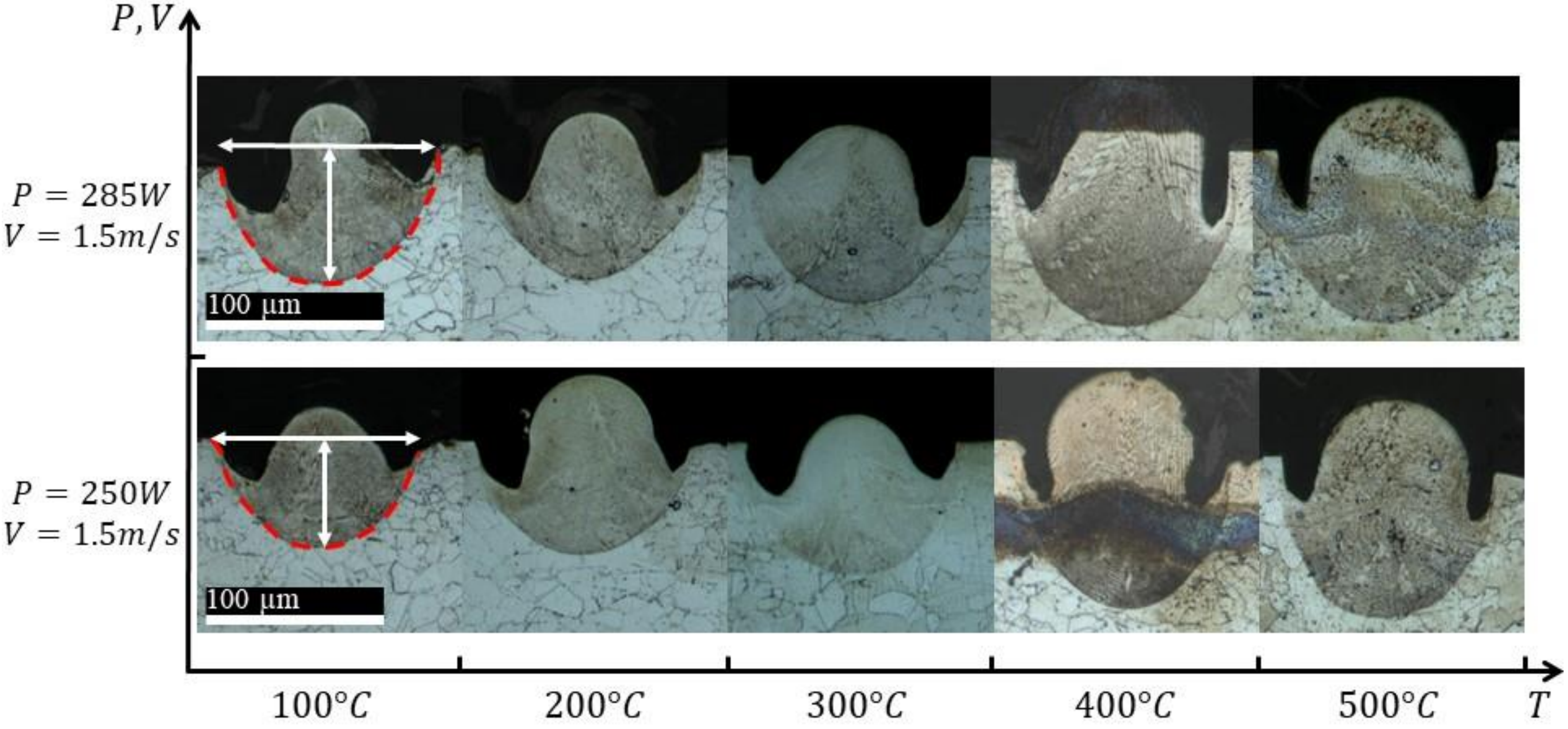

Melt pool in **conduction regime**

Experimental Measurements

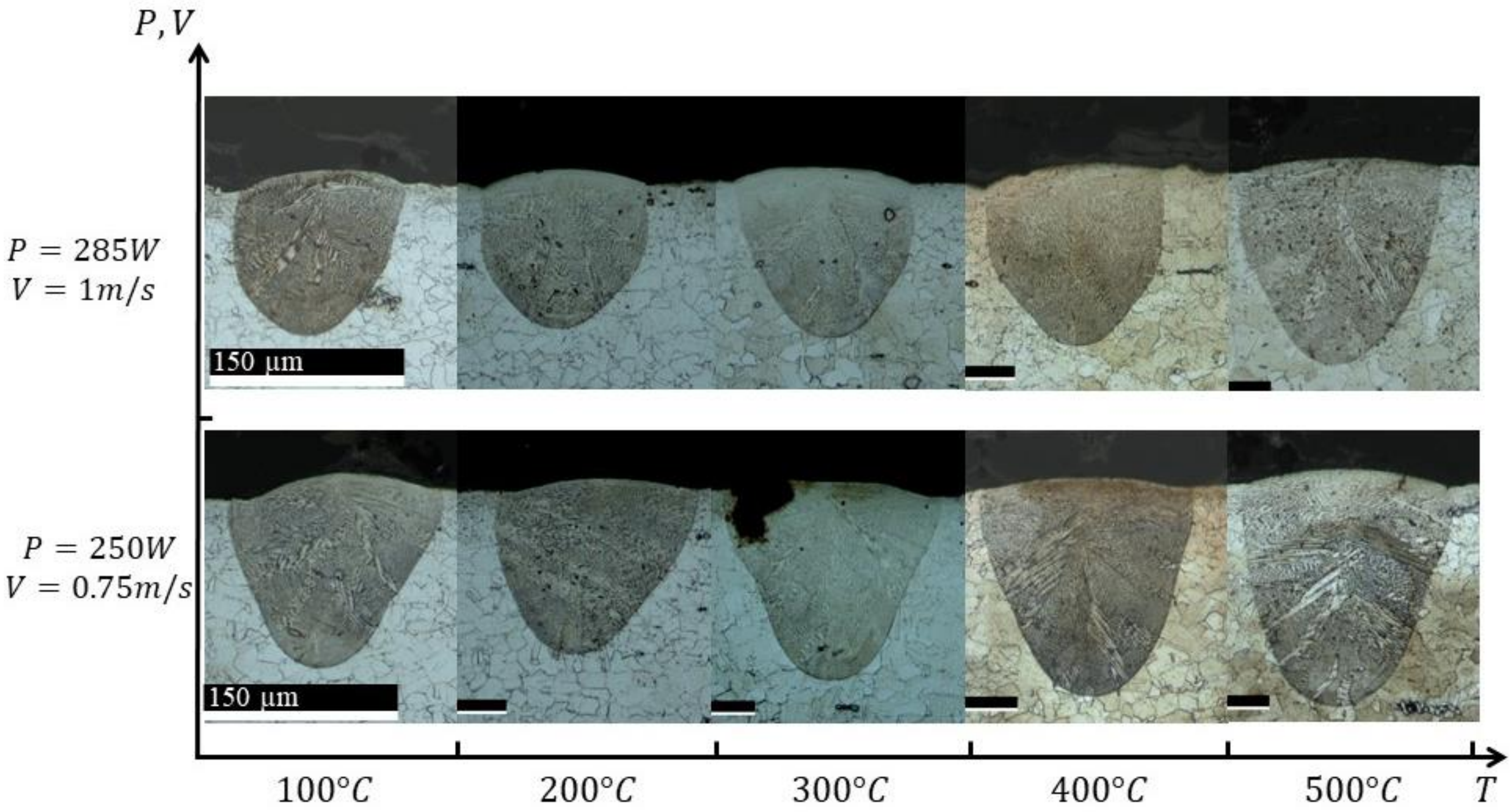

Melt pool in **transition regime**

Experimental Measurements

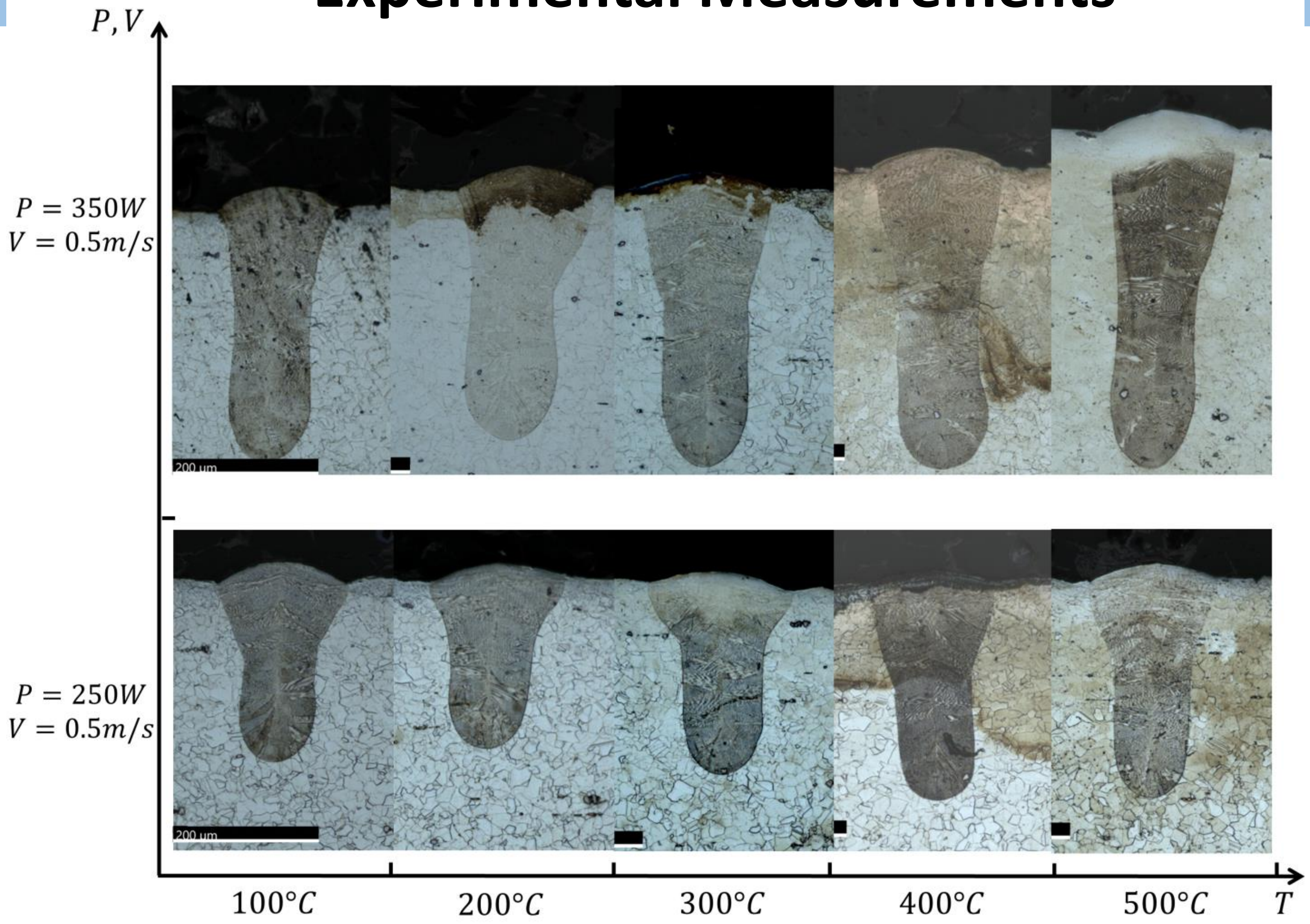

Melt pool in **keyhole regime**

Model Calibration

Conduction regime (P = 250 W and V = 1.5 m/s)

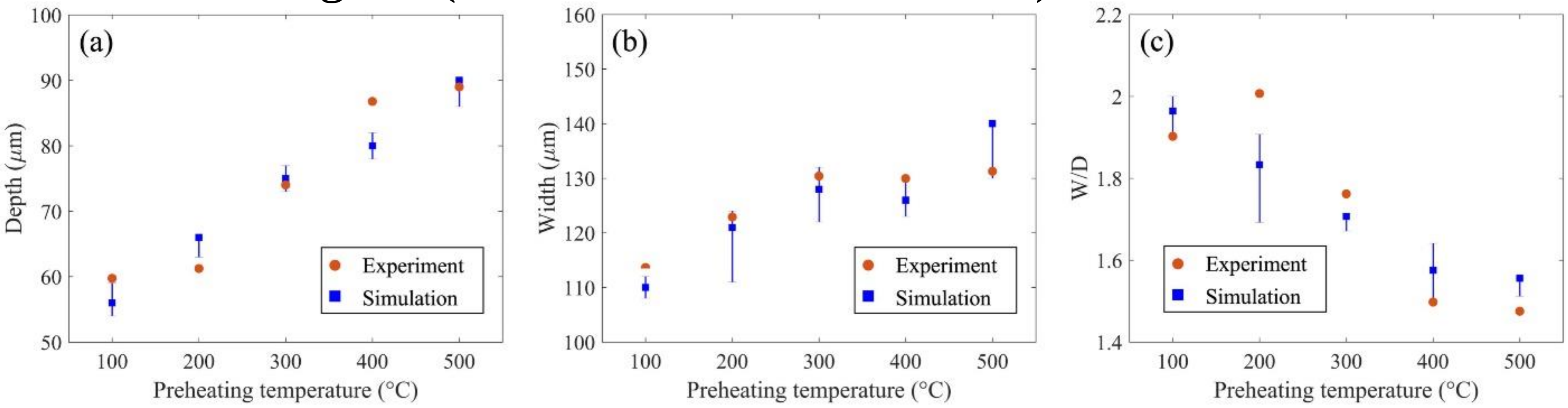

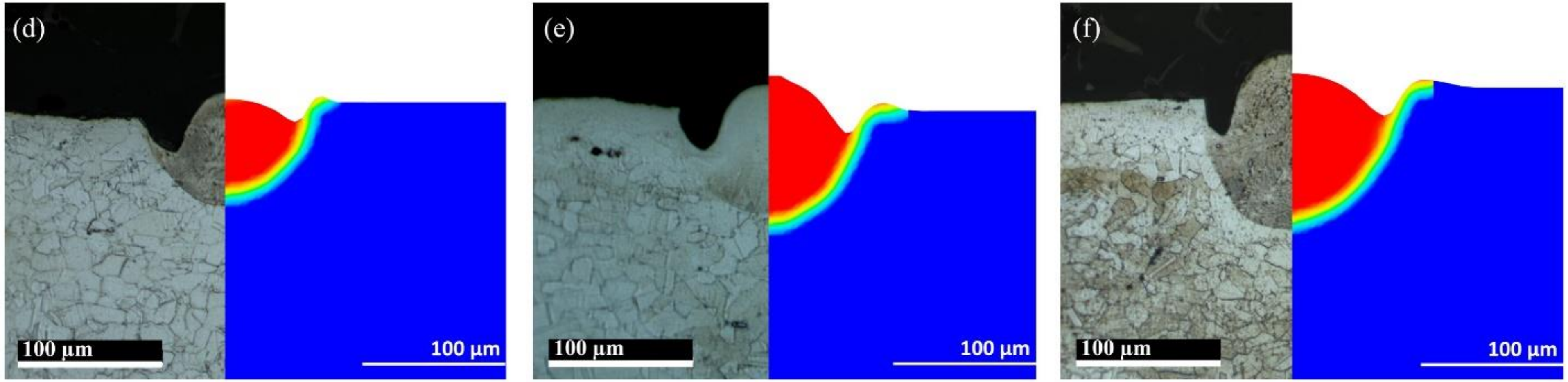

Preheating temperature: 100 °C

Preheating temperature: 300 °C

Preheating temperature: 500 °C

Model Calibration

Transition regime (P = 285 W and V = 1.0 m/s)

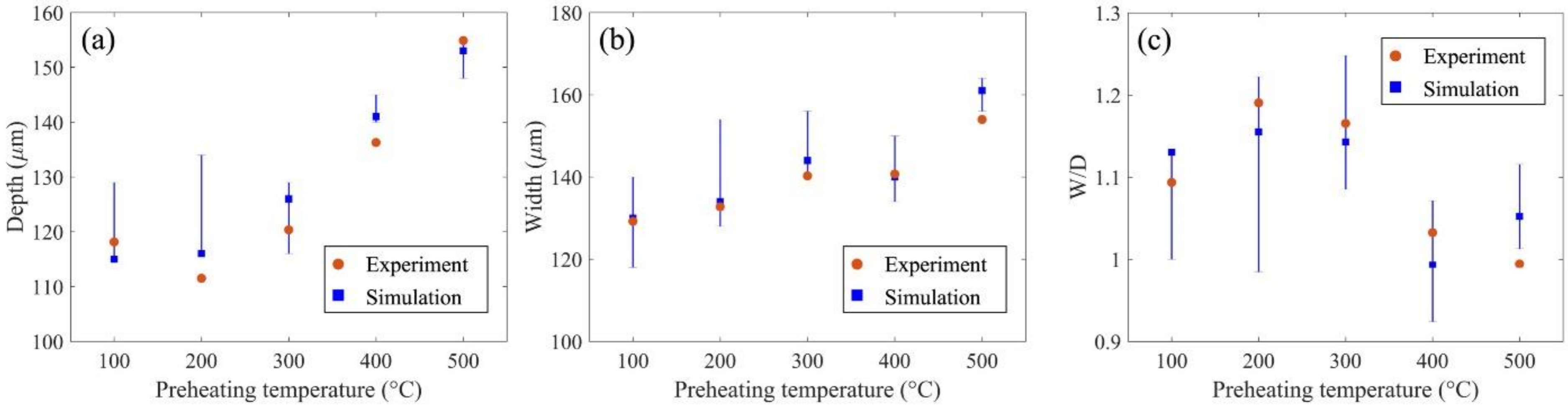

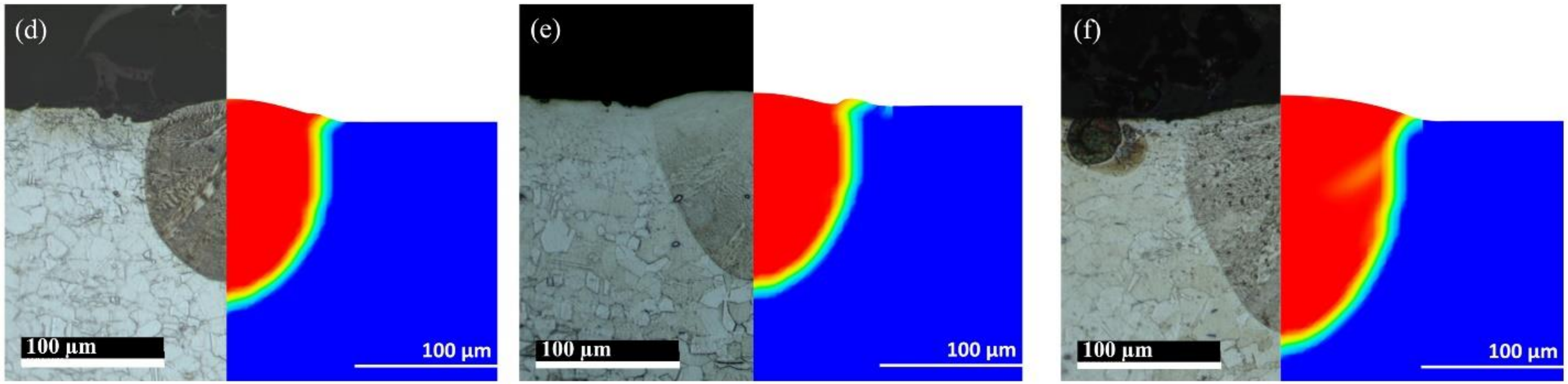

Preheating temperature: 100 °C

Preheating temperature: 300 °C

Preheating temperature: 500 °C

Model Calibration

Keyhole regime (P = 250 W and V = 0.5 m/s)

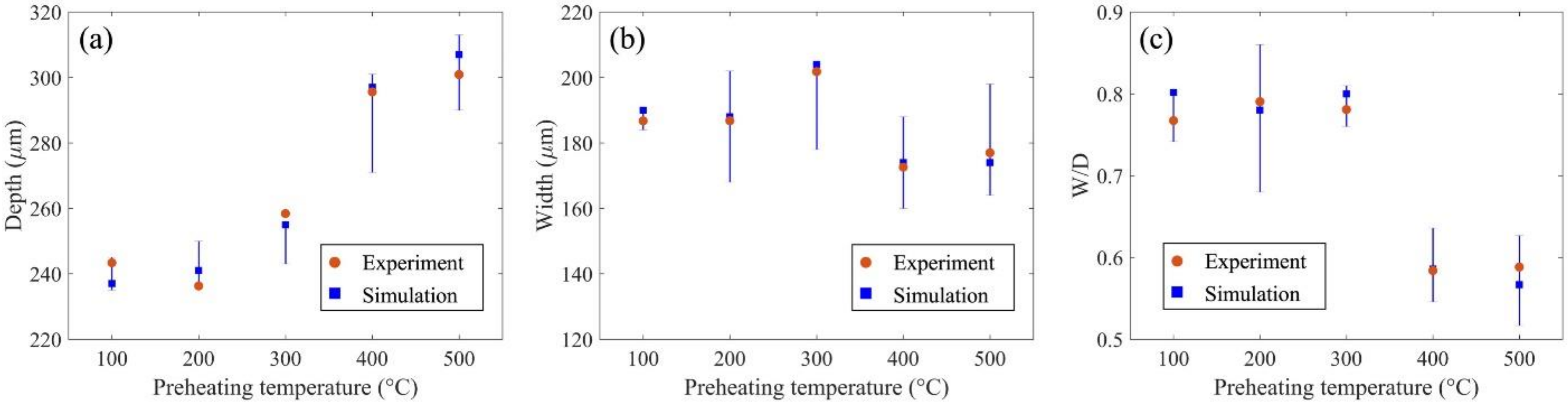

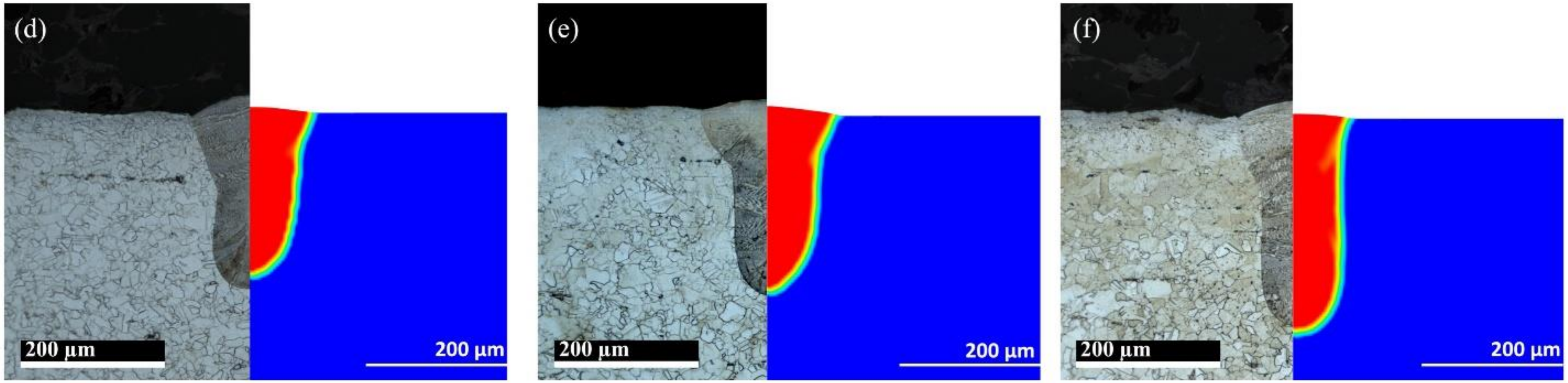

Preheating temperature: 100 °C

Preheating temperature: 300 °C

Preheating temperature: 500 °C

Temperature Dependent Material Properties

- Melt pool dimensions derived from analytical solution:

$$w = \sqrt{\frac{8}{\pi e} \cdot \frac{P\eta}{\rho C_p V (T_m - T_0)}}$$

$$d = w/2$$

P: power;
η: absorptivity;
ρ: density;
C_p: heat capacity;
V: scan speed;
T_m: melting point;
T_0: ambient temperature

Table1: Temperature dependent material properties of Inconel 718

Temperature (°C)	Density (g/cm3)	Capacity (J/Kg/°C)	k (W/m·°C)
100	8.16	455	10.8
200	8.118	479	12.9
300	8.079	497	15.2
400	8.04	515	17.4
500	8.001	527	18.7

M. Tang, P.C. Pistorius, J.L. Beuth, Prediction of lack-of-fusion porosity for powder bed fusion, Additive Manufacturing 14 (2017) 39-48.
P. Promoppatum, S.-C. Yao, P.C. Pistorius, A.D. Rollett, A comprehensive comparison of the analytical and numerical prediction of the thermal history and solidification microstructure of Inconel 718 products made by laser powder-bed fusion, Engineering 3(5) (2017) 685-694.

Temperature Dependent Material Properties

Table 2: Melt pool dimension in conduction regime comparison between analytical solution and experiment measurement ($P = 250\ W, V = 1.5\ m/s$ and $\eta = 0.4$)

Temperature (°C)	Width			Depth		
	Analytical solution (μm)	Experiment (μm)	Error (%)	Analytical solution (μm)	Experiment (μm)	Error (%)
100	118.4	113.66	4.17	59.2	59.74	-0.90
200	120.84	122.91	-1.68	60.42	61.24	-1.34
300	124.72	130.4	-4.36	62.36	74.01	-15.74
400	129.46	129.96	-0.38	64.73	86.78	-25.41
500	136.06	131.28	3.64	68.03	88.99	-23.55

Good agreement in width!!

Large error due to ignoring recoil pressure

$$P_s = A \cdot exp\left\{B\left(1 - \frac{T_v}{T}\right)\right\}$$

Conduction zone is still semicircular shape at 200 °C

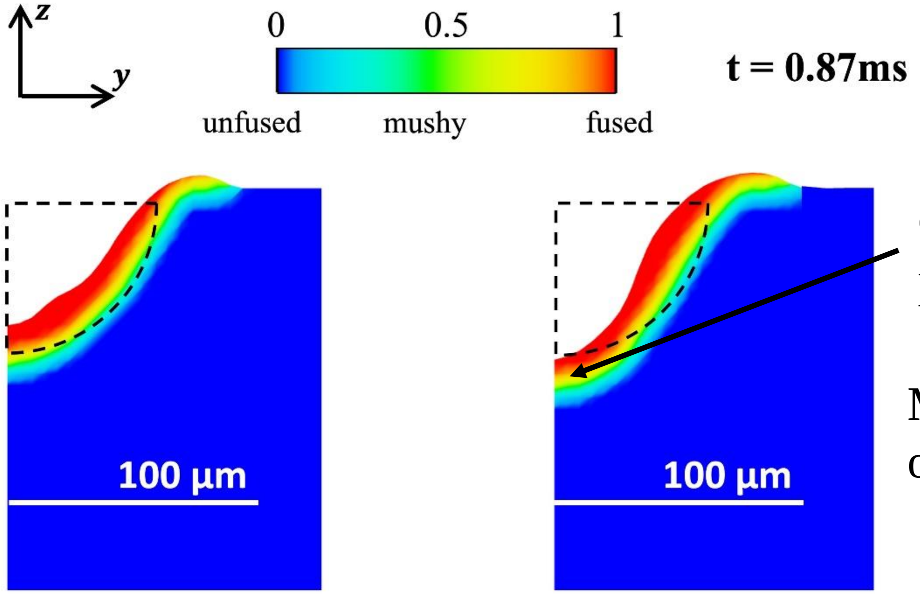

(a). Preheating temperature: 200 °C (b). Preheating temperature: 300 °C

Conduction zone gets penetrated at 300 °C

Melt pool depth depends on recoil pressure

Evaporation pressure and mass

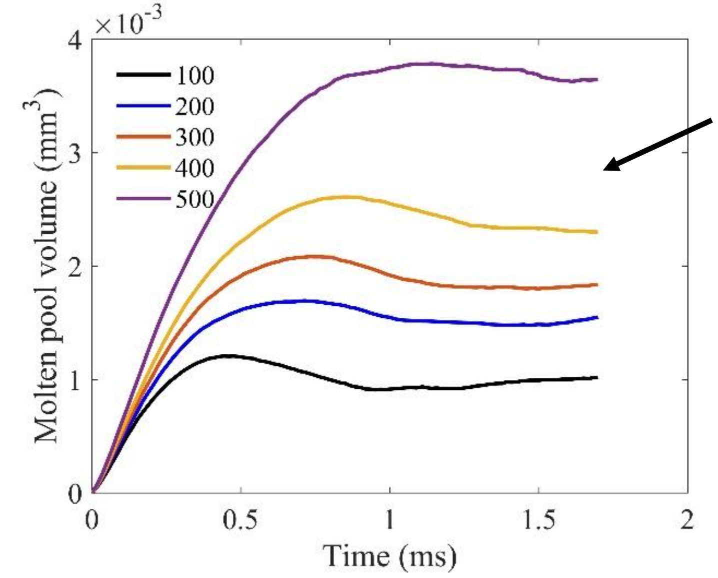

Conduction regime (P = 250 W, V = 1.5 m/s)

Molten pool volume change owing to material properties in conduction regime

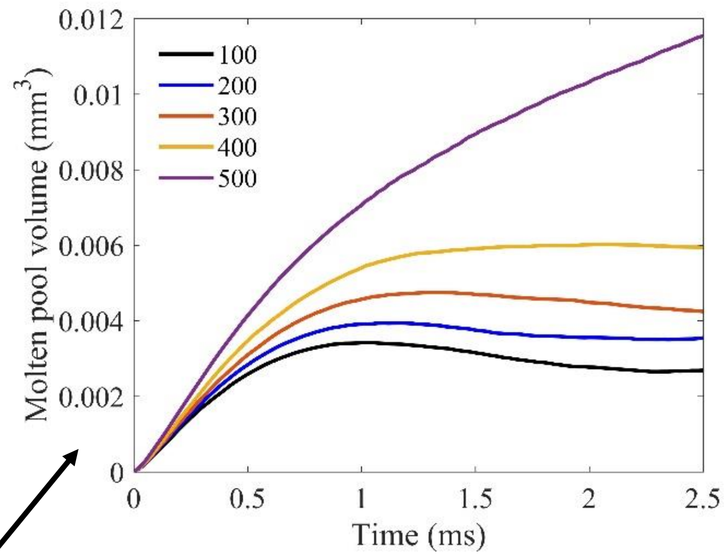

Transition regime (P = 285 W, V = 1.0 m/s)

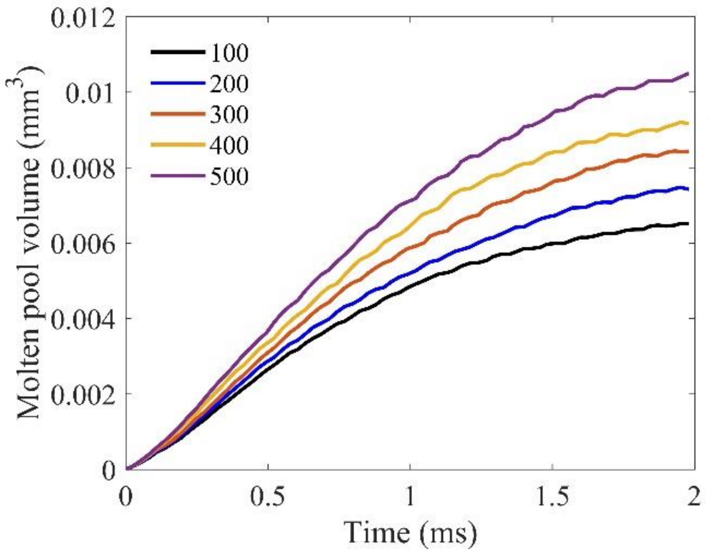

Keyhole regime (P = 250 W, V = 0.5 m/s)

Molten pool volume change owing to evaporation in transition and keyhole regime

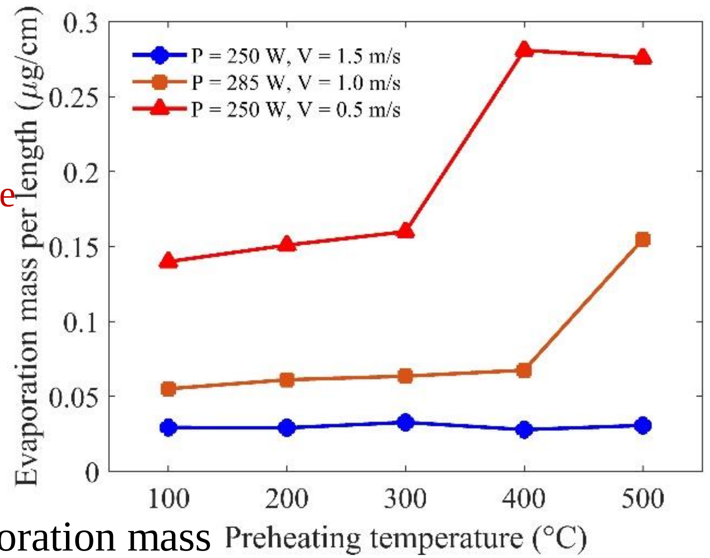

Evaporation mass

Laser Drill Rate

For melt pool in keyhole regime (P = 250 W, V = 0.5 m/s):

- Increasing the preheating temperature leads to deep melt pool
- Probability of porosity occurrence is increased at higher preheating temperature

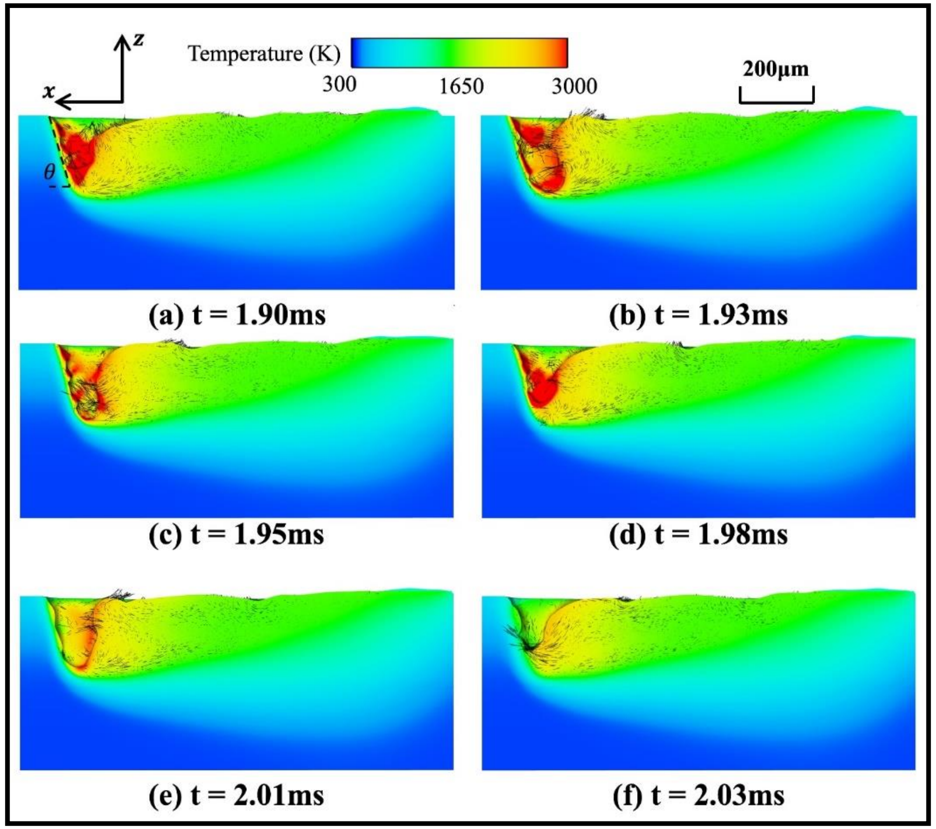

Preheating temperature: 100 °C

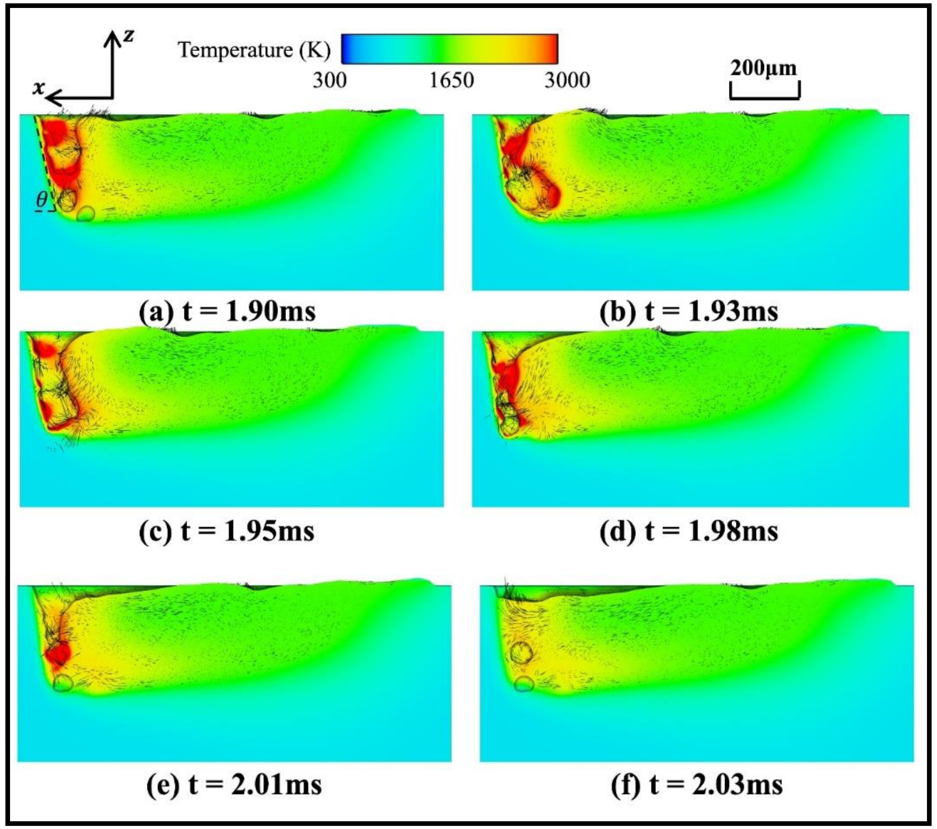

Preheating temperature: 500 °C

Laser Drill Rate

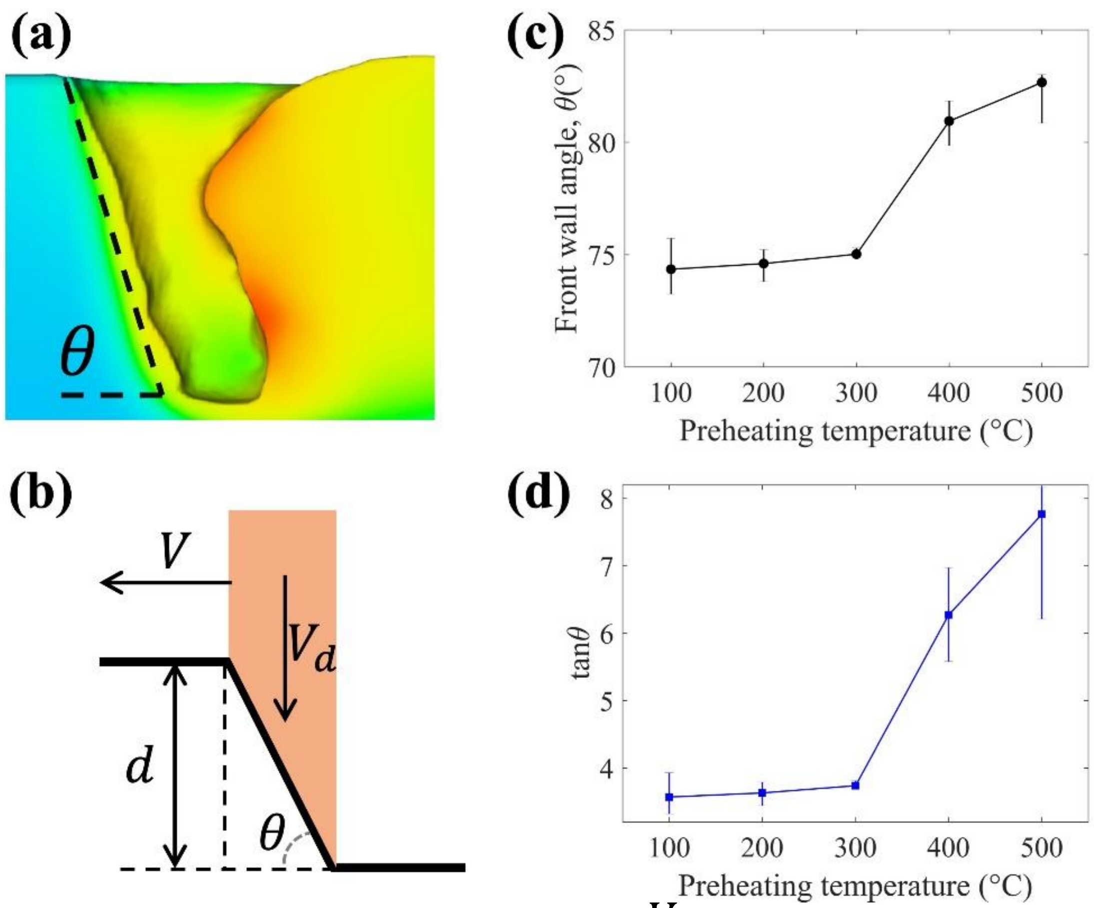

Laser drill rate V_d can be estimated by: $tan(\theta) = \frac{V_d}{V}$ Scan speed

Keyhole front wall angle

Laser drill rate at the preheating temperature of 500 °C (3.88 m/s) is 2.18 times larger than 100 °C (1.78 m/s)

R. Fabbro, K. Chouf, Keyhole modeling during laser welding, Journal of applied Physics 87(9) (2000) 4075-4083

Melt Track Length (conduction regime)

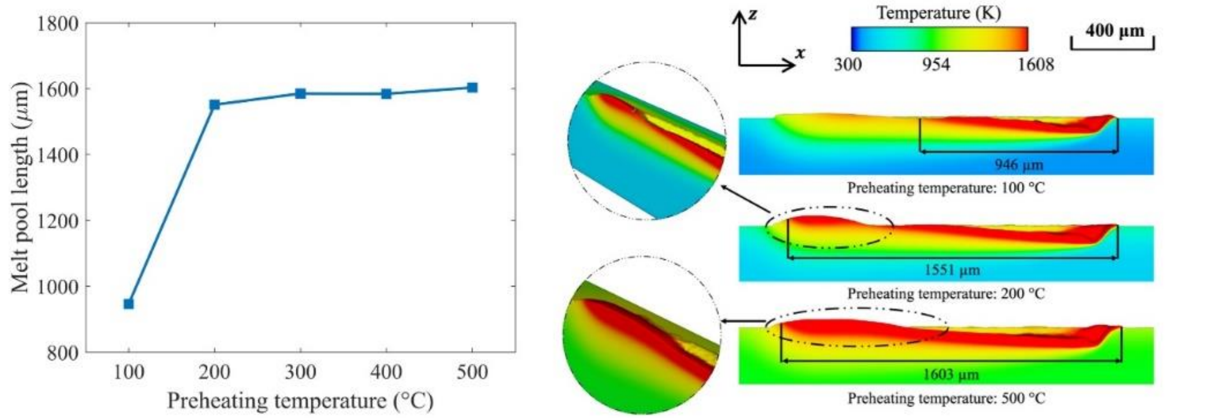

(a). Melt pool length variation at t = 1.00 ms (b). Simulation melt pool length at t = 1.00 ms

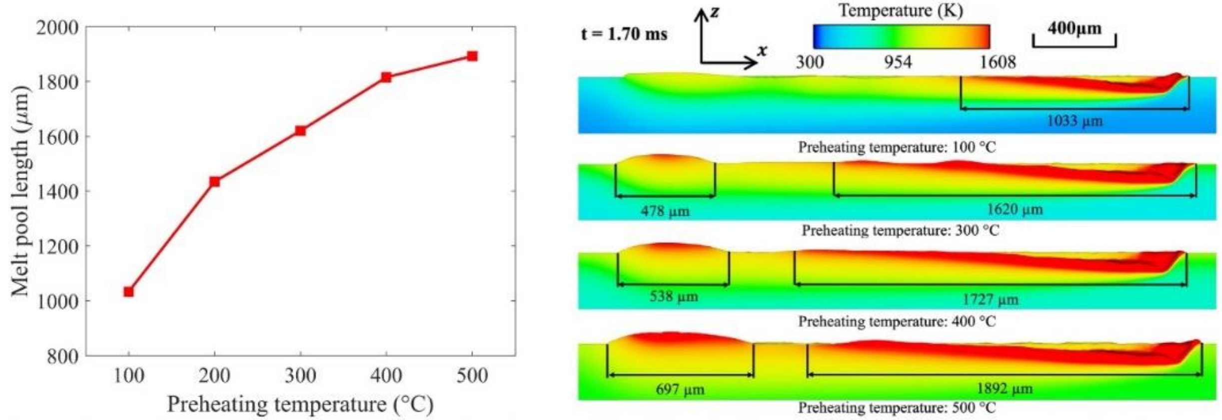

(c). Melt pool length variation at t = 1.70 ms (d). Simulation melt pool length at t = 1.70 ms

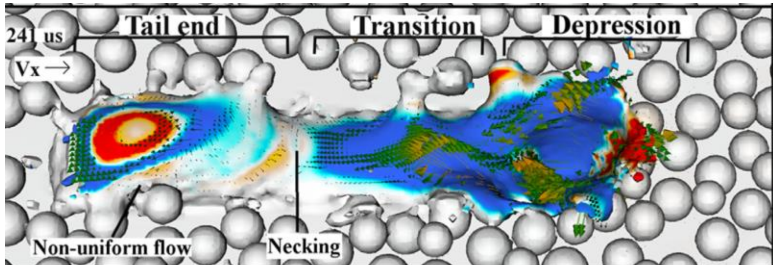

Khairallah, S. A., Anderson, A. T., Rubenchik, A., & King, W. E. (2016). Laser powder-bed fusion additive manufacturing: Physics of complex melt flow and formation mechanisms of pores, spatter, and denudation zones. *Acta Materialia, 108*, 36-45.

Melt Track Length

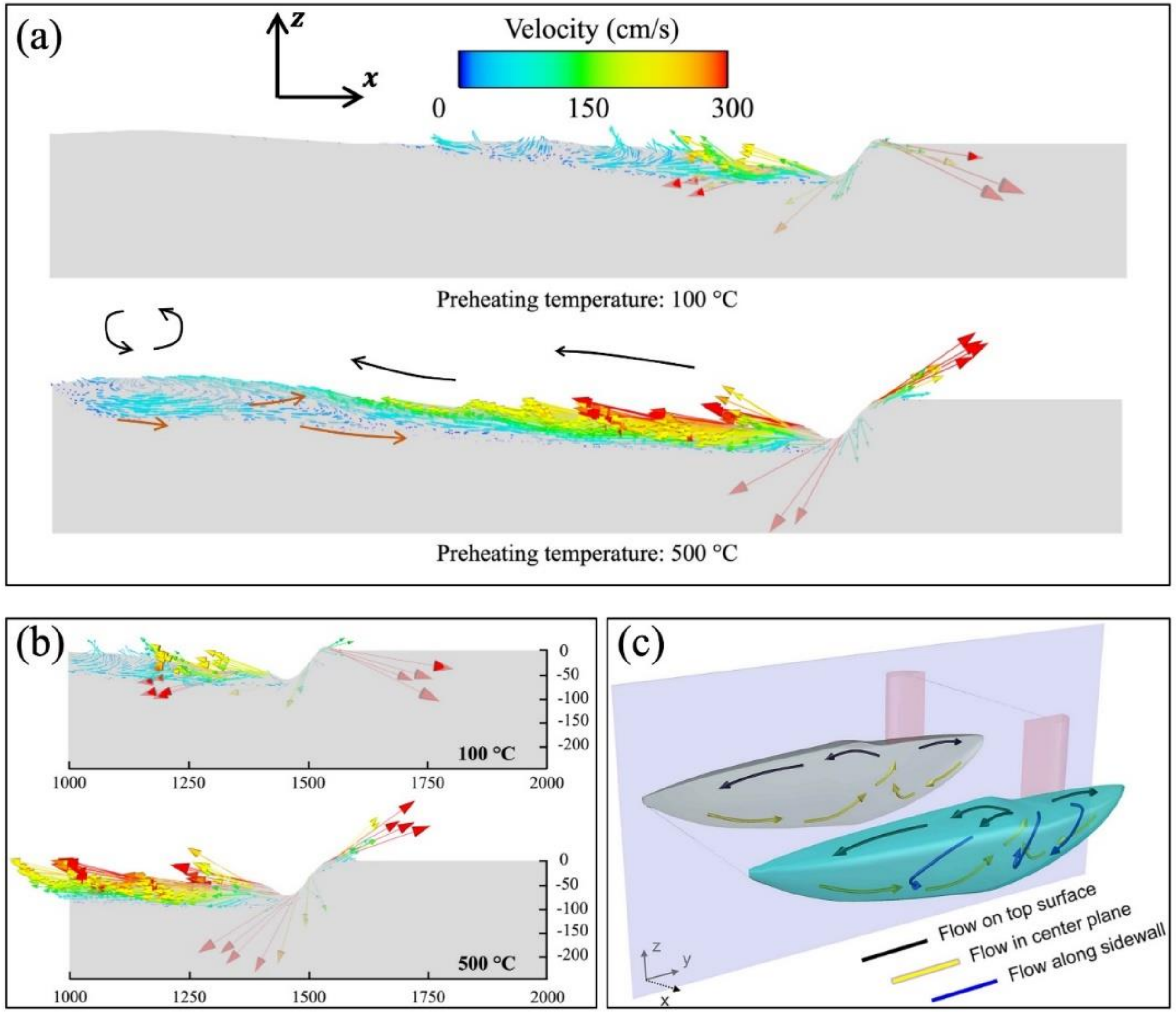

Q. Guo, C. Zhao, M. Qu, L. Xiong, S.M.H. Hojjatzadeh, L.I. Escano, N.D. Parab, K. Fezzaa, T. Sun, L. Chen, In-situ full-field mapping of melt flow dynamics in laser metal additive manufacturing, Additive Manufacturing 31 (2020) 100939

P-V and Preheating Process Map

- Conduction regime:

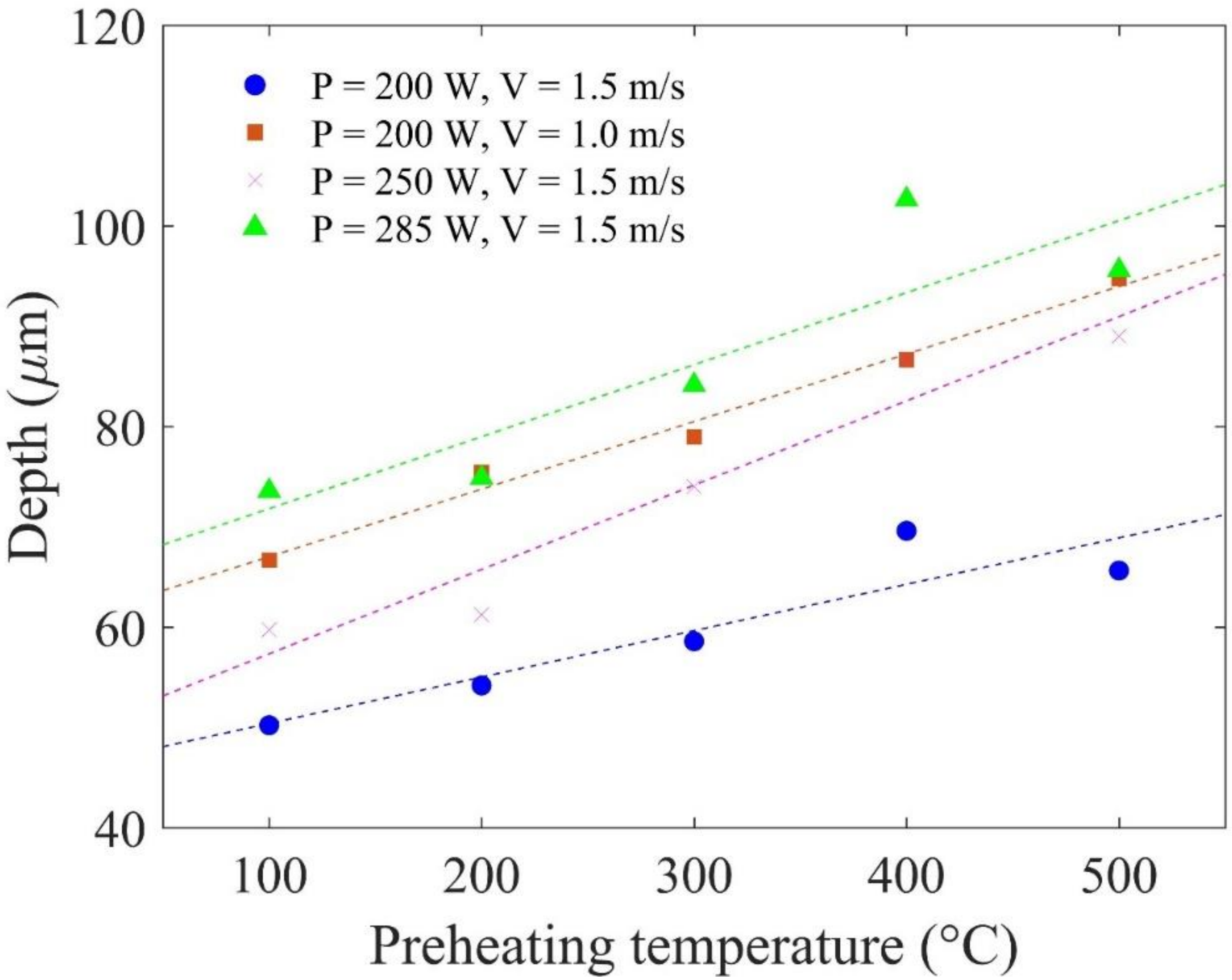

P-V and Preheating Process Map

- Transition regime:

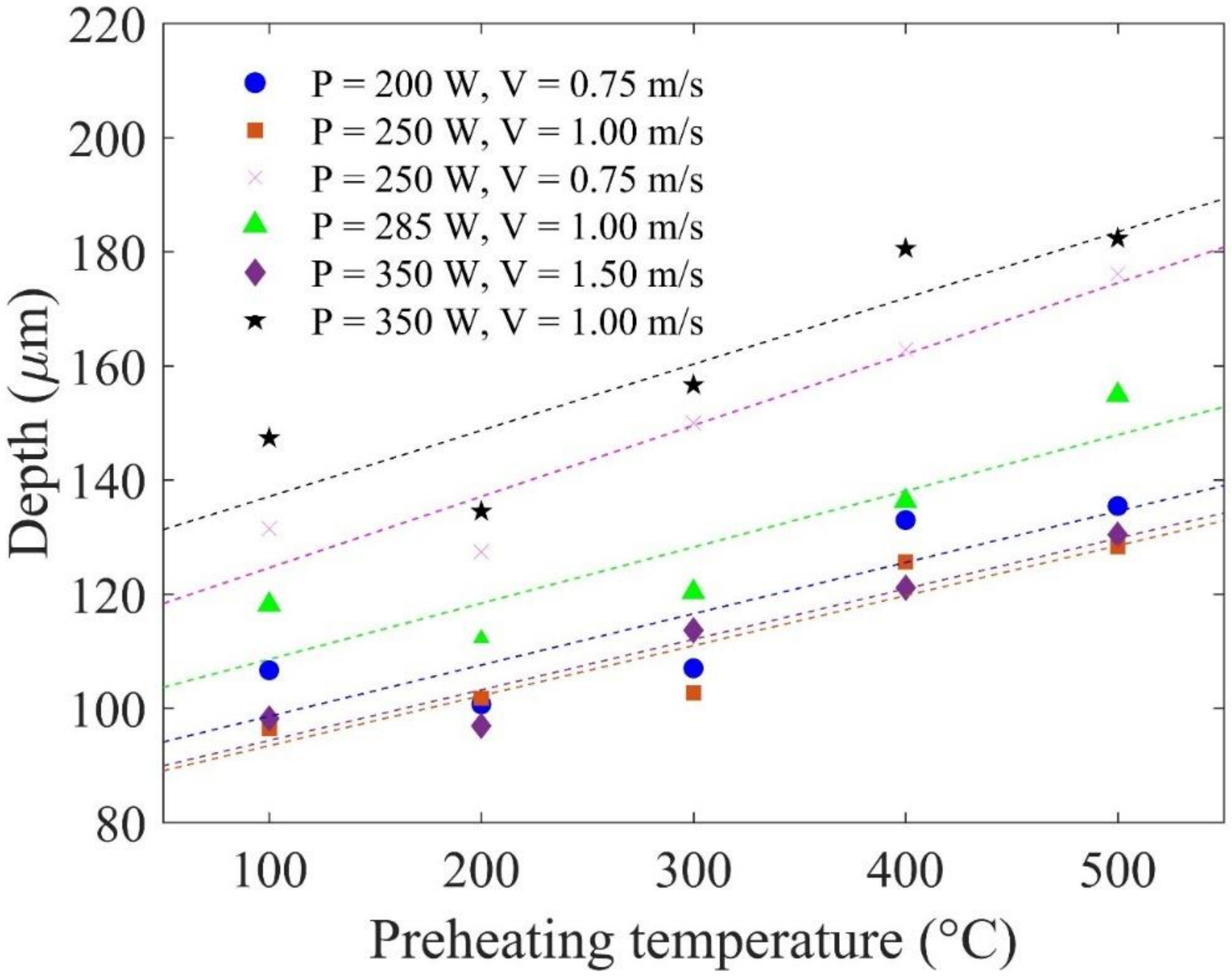

P-V and Preheating Process Map

- Keyhole regime:

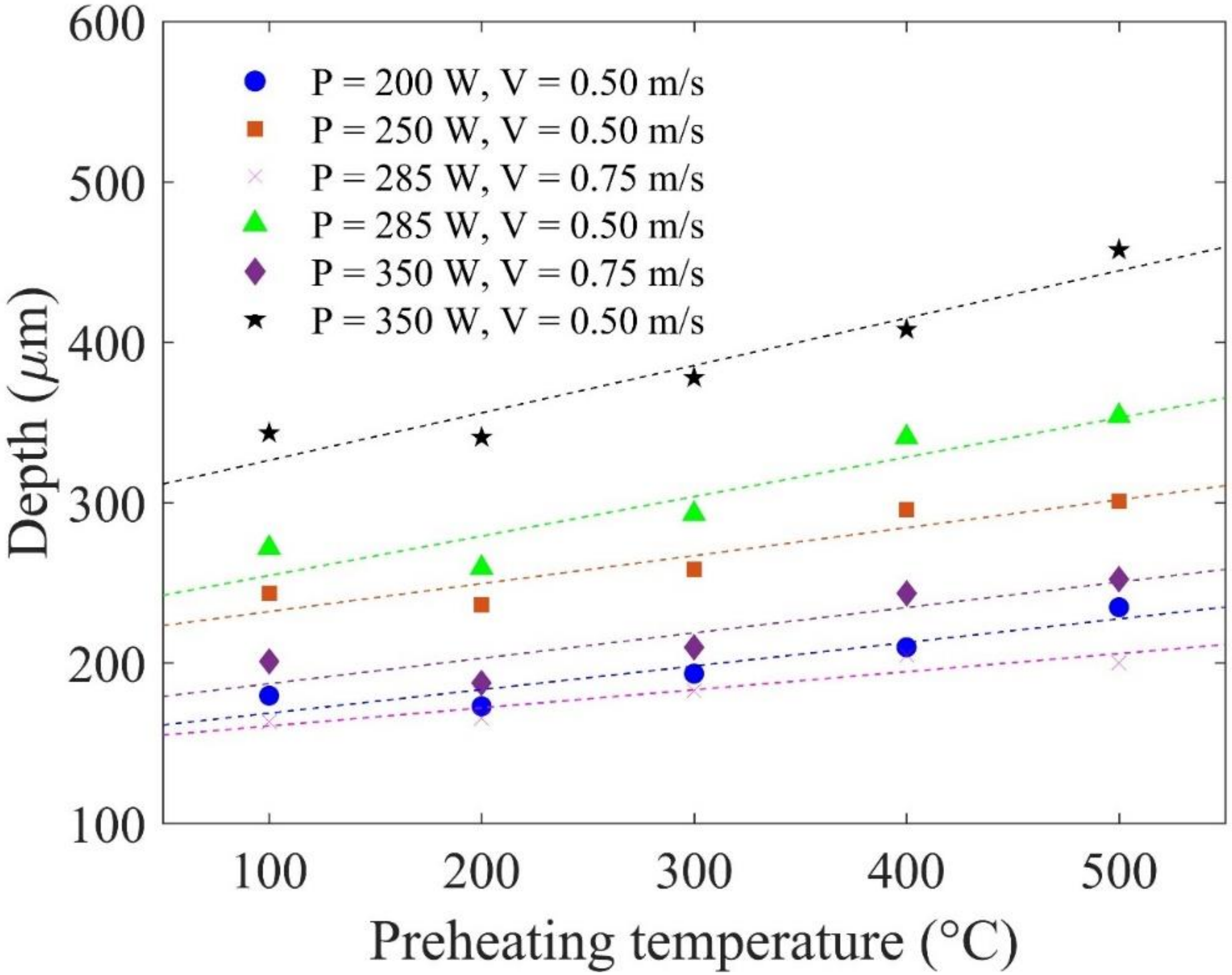

Conclusion

- The role of preheating temperature on melt pool morphology is confirmed by ex-situ experiments and numerical modeling.
- For melt pool in conduction regime, melt pool width and depth increase along with preheating temperature due to temperature dependent material properties; Recoil pressure becomes dominant at higher preheating temperature which makes the melt pool no longer semi-circular.
- In transition and keyhole regime, high preheating temperature leads to stronger mass evaporation which increases melt pool depth and molten pool volume.
- High preheating temperature also leads to stronger laser drill rate which gives rise to deep keyhole and incidents of porosity.
- Melt pool length also depends on preheating temperature since the rate and speed of backward flow from laser hot spot is related to the recoil pressure which is a function of preheating temperature.

Products

❖ Publications (1 Journal Paper, 2 Conference Paper)

1. Qian Chen, Yunhao Zhao, Seth Strayer, Yufan Zhao, Kenta Aoyagi, Yuichiro Koizumi, Akihiko Chiba, Wei Xiong, Albert To. Elucidating the effect of preheating temperature on melt pool morphology variation in Inconel 718 laser powder bed fusion via simulation and experiment. ***Additive Manufacturing (Accepted)***
2. Q. Chen, S. Strayer, A. C. To, "***Pore formation in laser powder bed fusion Inconel 718 through multiphysics modeling***“, Materials Science & Technology 2020, Virtual, November 2-6, 2020
3. Vallabh, C.K.P., Y. Xiong, and X. Zhao. ***In-situ Monitoring of Laser Powder Bed Fusion Process Anomalies via a Comprehensive analysis of off-axis Camera Data***. in *Proceedings of ASME 2020 International Manufacturing Science and Engineering Conference*. 2020. Cincinnati, Ohio, USA.
4. Note: PI’s group currently has 2 journal manuscripts in preparation (expected to publish in 2021).

❖ Inventions (1 Patent Application)

- Zhao, X., and Vallabh, C.K.P. (USPTO 17/015,062, filed on September 8, 2020) ***Systems and Methods of Adaptive Two-wavelength Single-camera Imaging Thermography (ATSIT) for Accurate and Smart in-situ Process Temperature Measurement during Metal Additive Manufacturing*** (University of Pittsburgh).

Dissemination to Communities of Interest

Time	Event & Venue	Primary Audience	Activity and Impact
11/2019	SciTech Exhibition at Carnegie Science Museum	K-12 Children	PI Zhao's group demonstrated metal 3D Printing and Computer Vision based monitoring technologies
03/2020	Women in 3D Printing – Pittsburgh Chapter Workshop at Pitt	Industry partners, University students	PI Zhao gave a presentation on "Additive Manufacturing Qualification" introducing part of this project research and results.
07/2020	ASPE (American Society of Precision Engineering) Summer Topical Workshop on Additive Manufacturing	ASPE members, including University and National Lab Researchers and industry attendees across the world	PI Zhao introduced and acknowledged this DOE NETL sponsored research project on in-situ monitoring and qualification of metal AM

Acknowledgement

- DOE NETL UTSR Program (Grant Number: DE-FE0031774)
- Project Manager: Mark C. Freeman
- University of Pittsburgh Swanson School of Engineering
- Co-PIs: Prof. Albert To (Pitt), Prof. Richard Neu (GaTech)
- PI Zhao's Research Lab (ZIP-AM)
  (Postdoctoral Fellow Chaitanya Vallabh,
  Graduate student Yubo Xiong)
- Industry Partners: Turbine Manufacturer, ANSYS